A CARD9-deficiency mouse model recapitulates human chronic CNS candidiasis identifying defective monocytic-cell responses in immunopathogenesis

Marija Landekic¹, Isabelle Angers^{2,3}, Yongbiao Li³, Marie-Christine Guiot⁴, Marc-André Déry³, Annie Beauchamp³, Lucie Roussel³, Annie Boisvert³, Wen Bo Zhou^{1,3}, Christina Gavino³, Julia Luo^{3,5} Stéphane Bernier³, Makayla Kazimerczak-Brunet³, Yichun Sun³, Brendan Snarr⁶, Michail S. Lionakis⁶, Robert T. Wheeler⁷, Irah L. King^{1,2}, Salman Qureshi², Maziar Divangahi^{1,2}, Donald C. Vinh^{1,3,5,8*}

¹ Department of Microbiology & Immunology, McGill University, Montreal, Quebec, Canada

² Meakins-Christie Laboratories, Department of Medicine, McGill University Health Centre, Montréal, Québec, Canada.

³ Infectious Disease and Immunity in Global Health, Research Institute of the McGill University Health Center, Montreal, Quebec, Canada

⁴ Department of Pathology, McGill University Health Center, Montreal, Quebec, Canada

⁵ Department of Human Genetics, McGill University, Montreal, Quebec, Canada

⁶ Fungal Pathogenesis Section, Laboratory of Clinical Immunology & Microbiology, National Institute of Allergy and Infectious Diseases, Bethesda, Maryland, USA

⁷ Department of Molecular & Biomedical Sciences, University of Maine, Orono, Maine, United States of America.

⁸ Department of Medicine, Division of Infectious Diseases, McGill University Health Centre, Montréal, Québec, Canada.

^{*}Corresponding author: Donald C. Vinh, RI-MUHC, 1001 Décarie Blvd., EM3-3211, Montréal, Quebéc, Canada H4A 3J1. Phone: +1.514.934.1934 ext. 42419; Email: donald.vinh@mcgill.ca.

Conflict of Interest Statement: The authors have declared that no conflict of interest exists.

Abstract

Human Caspase Recruitment Domain Containing Protein 9 (CARD9) deficiency predisposes to invasive fungal disease, particularly by *Candida* spp. Distinctly, CARD9-deficiency causes chronic central nervous system (CNS) candidiasis. Currently, no animal model recapitulates the chronicity of disease, precluding a better understanding of immunopathogenesis. We established a knock-in mouse homozygous for the recurring p.Y91H mutation (Y91H^{KI}) and, in parallel to Card9^{-/-} mice, titrated the intravenous fungal inoculum to the CARD9-genotype to develop a model of chronic invasive candidiasis. Strikingly, CARD9-deficient mice had predominantly CNS involvement, with neurological symptoms appearing late during infection and progressive brain fungal burden in the absence of fulminant sepsis, reflecting the human syndrome. Mononuclear cell aggregation at fungal lesions in the brain correlated with increased MHCII⁺Ly6C⁺ monocyte numbers at day 1 post-infection in WT and Y91H^{KI} mice, but not in Card9^{-/-} mice. At day 4 post-infection, neutrophils and additional Lv6C⁺ monocytes were recruited to the CARD9-deficient brain. As in humans, Y91HKI mutant mice demonstrated cerebral multinucleated giant cells and granulomata. Subtle immunologic differences between the hypomorphic (p.Y91H) and null mice were noted, perhaps explaining some of the variability seen in humans. Our work established a disease-recapitulating animal model to specifically decipher chronic CNS candidiasis due to CARD9 deficiency.

Introduction

Inborn errors of immunity in Caspase Recruitment Domain Containing Protein 9 (CARD9) lead to spontaneous development of invasive fungal disease in humans, particularly of the central nervous system (CNS) with *Candida albicans* (1). CARD9 deficiency is caused by loss-of-function mutations, ranging from complete loss of protein expression to hypomorphic missense mutations, and is inherited in an autosomal recessive pattern. The recurring c.T271C (p.Y91H) mutation has been reported in 6.7% of CARD9-deficient patients (2, 3), but how this missense substitution leads to invasive candidiasis is still poorly understood (2, 4).

Commonly-used models of candidiasis in mice rely on pharmacologically induced fungal colonization and dissemination, either by antibiotic or corticosteroid treatment, use of anti-cancer agents that suppress the immune system, or a combination of these strategies (5, 6). These preclinical models reflect the human form of iatrogenic invasive candidiasis, providing great insight into acute fungal disease associated with malignancy (7). However, invasive fungal disease in CARD9-deficiency is spontaneous (i.e. in the absence of exogenous immunosuppression) and indolent; thus, the conventionally-used experimental approaches do not accurately model this specific human condition. Consequently, these aforementioned mouse models preclude our understanding of CARD9-dependent mechanisms underlying host antifungal defenses, particularly in the CNS. A model of candidiasis that accurately recapitulates human CARD9 deficiency is invaluable to decipher its immunopathogenesis.

CNS involvement has been studied as an extension of multi-organ disease (disseminated candidiasis) in mice with candidemia (8, 9). This latter approach typically uses an inoculum ranging 10⁴-10⁶ colony forming units (CFU) of *C. albicans* yeast cells in C57BL/6 mice delivered by intravenous (I.V.) injection. Wild-type (WT) mice that succumb to infection at these

doses die of progressive sepsis and kidney failure (10, 11); on necropsy, neutrophil-mediated kidney immunopathology is apparent, as is damage to other organs, including the brain (10, 12, 13). These studies have shown that myeloid cells, namely neutrophils, monocytes, and tissueresident macrophages, are essential for tissue protection, as ablation or inhibition of any of these cells increases mortality in mice (10, 14, 15). Using this model, Card9^{-/-} mice show that the early neutrophil infiltration into the brain (24 hours post-infection, P.I.) is essential to control fungal growth, as impaired neutrophil trafficking enhances disease (9). However, as invasive candidiasis associated with human CARD9 deficiency is often chronic in nature, with a median age at onset of 17.5 years (range 3.5-58 years) (1, 16), and is not typically accompanied by fulminant sepsis, the relevance of these mouse models to understanding the chronic features of the human disease remains unclear. By using WT mice, but infected with a lower fungal inoculum, a recent study has also demonstrated that mononuclear phagocytes, including brainresident macrophages (microglia) and monocytes, play a key role in limiting tissue fungal burden by forming "fungus-induced glial granuloma" in the absence of neutrophil infiltration (17). Importantly, the immune response of CARD9-deficient mice at lower doses may also diverge from the response reported using the acute sepsis model of candidemia. Therefore, a preclinical system that more closely models the clinical presentation of CARD9-deficiency in humans would provide an experimental platform to better understand the mechanisms by which CARD9 mediates anti-Candida immunity, and for development of therapeutic strategies.

In this study, we used CRISPR-Cas9 technology to generate a knock-in mouse homozygous for the c.T271C (p.Y91H) mutation (Y91H^{KI} mice). By titrating the *C. albicans* inoculum to the CARD9 genotype, we established a clinically-pertinent CARD9-deficient model of chronic invasive candidiasis that recapitulates distinct clinical and histopathological features

of the human CNS disease, including primarily neurological symptoms, occasional skull destruction, and granulomatous-like inflammation during late-stage infection. At a systemic level, the Y91H^{KI} mice phenocopy *Card9*^{-/-} mice in terms of survival, dissemination, and tissue fungal burden, confirming that the homozygous p.Y91H mutation is sufficient for fungal disease. At the level of host defense, Y91H^{KI} neutrophil anti-candidal functions parallel those of *Card9*^{-/-} neutrophils. By tracing the kinetics of both tissue fungal growth and the myeloid response in the brain, we identify the critical role of mononuclear phagocyte responses to fungal infection in the brain. Specifically, our data implicate MHCII⁺Ly6C⁺ monocyte-derived cells (moDC) as early responders to CNS fungal invasion. The development of a CARD9-dependent chronic invasive candidiasis murine model that better emulates human CARD9 deficiency provides a framework to decipher the disease's immunopathology and potentially direct the development of mechanism-based intervention strategies.

Results

Knock-in of the human p.Y91H mutation in mice.

To understand how the p.Y91H mutation in CARD9 predisposes to invasive candidiasis, we used CRISPR/Cas9 to knock-in the c.T271C mutation into C57BL/6N mice (Supplementary Figure 1A). Mice were bred to homozygosity to generate a CARD9^{c.T271C/c.T271C} homozygous knock-in mouse (Y91H^{KI}). All genotyping was confirmed by Sanger sequencing (Figure 1A). We initially evaluated Card9 expression in Card9^{-/-} (C57BL/6J background) and Y91H^{KI} bone-marrow derived macrophages (BMDM) by RT-PCR (Fig. 1B) and western blot (Figure 1B). C57BL/6J and C57BL/6N were used as controls for the genetic background of each mutant mouse throughout our investigations. Card9-/- BMDM show a loss of expression at both the mRNA and protein level. Y91HKI BMDM retained expression of CARD9 at both the transcript and protein levels, consistent with monocytes from CARD9^{p.Y91H} patients (4, 18). Using flow cytometry, we first performed immunophenotyping of the myeloid compartment of the bone marrow, blood, spleen, brain and kidney at steady state (Supplementary Figure 1B-D) and found no differences between the knock-out, knock-in, or WT mice. These data support previous studies indicating CARD9 is redundant for myeloid cell development and homeostasis in mice at steady state (19), and the absence of overt myeloid cell deficiencies in CARD9 deficient patients (1, 16, 20). Thus, the Y91H^{KI} mouse is a newly-developed tool to potentially understand the immunological mechanisms by which CARD9 regulates susceptibility to candidiasis.

Y91HKI mice phenocopy Card9-/- mice during disseminated candidiasis in vivo.

To begin investigating the *in vivo* consequences of the p.Y91H mutation, mice were infected intravenously (IV) with $1x10^5$ yeast cells, a standard model of disseminated candidiasis (9, 11,

13, 14, 21). Mice were then monitored for morbidity (weight loss) and survival (Figure 1C, D). In this high-dose model, Y91H^{KI} mice succumbed to infection within 7 days. The survival of Y91H^{KI} mice was slightly longer than *Card9*-/- mice, but did not reach statistical significance. Heterozygous mice displayed an intermediate susceptibility within the 30-day survival experiment. There was no difference in survival between the two CARD9 WT mice, showing that any genetic differences between these related strains do not affect survival outcome during infection with high-dose disseminated candidiasis. Thus, Y91H^{KI} mice phenocopy *Card9*-/- mice during high-dose infection with respect to acuity, morbidity, and mortality, demonstrating that this protein residue is essential for CARD9 function in mice.

The p.Y91H mutation results in enhanced fungal growth and susceptibility to disseminated disease.

As lethality during disseminated candidiasis is correlated to kidney fungal burden in WT mice (21), and *Card9*^{-/-} mice fail to control fungal growth not only in the kidneys but also in the brain (9, 11), we next compared the kinetics of tissue fungal burden in both kidney and brain (Figure 2). As a control, the fungal burden was also assessed in the spleen, since it is not considered a primary target organ for uncontrolled fungal growth during invasive candidiasis in non-neutropenic hosts (11, 21) (Supplementary Figure 2A). Fungal growth at day 1 P.I. in CARD9-deficient mice is comparable to WT mice, suggesting that initial seeding of *C. albicans* from the blood into the tissues was similar (Figure 2A, B). However, the fungal burden was significantly increased in CARD9-deficient mice in the kidney at day 2, and in the brain after day 3 post-infection (Figure 2A, B). Together, these data suggest that the initial hematogenous seeding of

C. albicans into target organs is subsequently restrained in WT mice, whereas Y91H^{KI} and *Card9*-/- mice fail to control it, resulting in extensive fungal growth within these tissues.

Histopathology analysis of Y91H^{KI} revealed extensive fungal lesion formation and hyphal filaments (Figure 2C), consistent with published data showing hyphal formation in *Card9*^{-/-} mice at the same time point (9). At day 3 post-infection, the burden in the spleen of both CARD9-deficient mouse strains significantly increases, and this time point coincides with the onset of mortality (Supplementary Figure 2A). WT mice show no significant increase in spleen burden or mortality within this time frame. Thus, in this high-dose candidiasis model, Y91H^{KI} phenocopy *Card9*^{-/-} tissue susceptibility at three non-contiguous anatomical locations, suggesting that these mice have comparable defects in antifungal defenses.

A model of chronic CNS candidiasis caused by CARD9-deficiency.

Fulminant morbidity and mortality, as well as the disseminated (multi-organ) nature of candidiasis observed in the CARD9-deficient strains using the high-dose approach, poorly models the fungal disease in human CARD9-deficiency, where disease can progress over years with predominant CNS involvement and pauci-involvement of other organs (1, 3, 4). We hypothesized that a fungal dose tailored to the CARD9-deficient state may permit a better understanding of the clinically-relevant processes critically regulated by CARD9. Dose response experiments in the Y91H^{K1} mouse revealed an LD₅₀ < 1x10³ yeast cells in a 30-day period, i.e. over 2-log₁₀ fold lower than in WT mice (Figure A). Unlike the high-dose inoculum (1×10^5) yeast cells), which induced end-point/terminal disease as early as 3 days P.I., both CARD9-deficient genotypes infected intravenously with the low-dose inoculum (1×10^3) yeast cells) only began reaching endpoints more than one week after inoculation (Figure 3B). Weight loss is statistically

significant but small in CARD9-deficient mice within the first week of infection (Supplementary Figure 2B); thus, severe morbidity is absent during this time compared to the high-dose model (Figure 1C). These findings indicate that infection with the low-dose *C. albicans* inoculum, which results in complete survival of WT mice, causes an indolent form of candidiasis in the CARD9-deficient mice, mimicking the chronicity of fungal disease observed in human CARD9 deficiency.

Dissecting host-pathogen responses in the brain is difficult in the high-dose model of disseminated candidiasis because mice rapidly develop sepsis and die from kidney involvement (Figure 2B) (10-12). We capitalized on our chronic model to investigate these responses. Firstly, we evaluated the kinetics of fungal growth in the brain by colony forming unit (CFU) assay (Figure 3C). At day 1 P.I., the fungal burden was the same among all groups (Supplementary Figure 2C, D). WT mice clear C. albicans from the brain to the level of detection by day 3 P.I. In contrast, there is an increasing fungal burden in CARD9-deficient mice up to day 9 P.I., when mice began reaching end-point. Card9^{-/-} brain burden on day 9 P.I. trends higher than that seen in Y91HKI mice, although the difference was not statistically significant. When comparing tissue fungal burden of Y91HKI mice with Card9-/- mice in this chronic model (Figure 3C), Y91HKI mice phenocopy Card9^{-/-} mice in the kinetics and scale of fungal burden in the brain. Overall, these results not only confirm that loss of CARD9 function confers susceptibility to invasive candidiasis, but that it does so by decreasing the threshold of C. albicans inoculum required to cause disease. Moreover, the comparability in brain fungal burden data between CARD9deficient mouse genotypes confirms their suitability to study chronic invasive CNS candidiasis.

Despite similarities in LD₅₀ and tissue involvement with brain proclivity, differences in disease manifestations were observed during the 30-day survival experiment between the

Y91H^{KI} and *Card9*^{-/-} mice (Figure 3D, and Supplementary Videos 1 and 2). Both genotypes displayed overt neurological symptoms, such as altered gait or head tilting late in infection. All mice that displayed symptoms reached the endpoint criteria (Figure 3E). Of the Y91H^{KI} mice that reached endpoint, 50% displayed neurological symptoms. The *Card9*^{-/-} mice displayed a more severe phenotype, as 66% of mice that reached the endpoint developed skull deformation (Figure 3D, E). One third of the *Card9*^{-/-} mice that reached the endpoint displayed neurological symptoms first, then progressed to skull deformation and severe morbidity. Another third had no observed behavioral changes but progressed to skull distention. These necropsy observations were confirmed by CT scan showing that the skull had distended in these mice (Figure 3D). Taken together, these results show that, while both CARD9-deficient mouse strains develop chronic CNS candidiasis with increasing brain fungal burden, *Card9*^{-/-} mice develop a more severe phenotype (skull deformity) late in infection.

CARD9-deficient mice display a progressive inflammatory response in the brain.

To better understand the immunopathogenesis of chronic invasive candidiasis in CARD9-deficient mice, we performed histopathology over the course of disease. Grocott-Gomori's methenamine silver (GMS) stain for fungus was performed on serial brain sections, along with hematoxylin and eosin (H&E) staining, to correlate areas of fungal lesions with cellular responses (Figure 4 and 5 and Supplementary Figure 3 and 4). No histological differences were observed between non-infected WT and CARD9-deficient mouse brains. One day P.I., mice displayed sparse fungal staining, consistent with the low abundance of CFU detected. Fungal lesions increased in number and size at day 4 and day 7 in CARD9-deficient brain, but not in WT mice (Figure 4B). As early as day 1 P.I. in Y91H^{KI} mice, inflammatory lesions at sites of

fungal staining were observed, becoming more apparent at days 4 and 7 P.I. in both CARD9-deficient strains. From day 4 P.I. onward, as no fungal lesions were detected by GMS in WT samples, images shown were aligned with anatomical locations of fungal lesions from CARD9-deficient samples. By day 7 P.I., robust inflammation and hyphae can be observed in several areas from the ventral striatum to the midbrain and pons.

Detailed analysis of fungal lesions at day 1 P.I. showed yeast and hyphal morphology in both WT and Y91H^{KI} mice, and H&E staining revealed cell aggregates clustering at fungal lesions (Supplementary Figure 3). Fungal lesions detected at day 4 P.I. in CARD9-deficient mice were larger than those observed at day 1 P.I. (Supplementary Fig 4). By day 7 P.I., CARD9-deficient mice showed extensive granulomatous inflammation throughout the brain as well as multinucleated giant cells (Fig 5). These histological findings were also noted in the brain biopsies of CARD9-deficient patients bearing p.Y91H (Fig 5 d). Interestingly, *Card9*-/- mice showed large granuloma formation surrounding a thick fungal mass, as well as multiple smaller granulomata throughout the brain. Granulomata in Y91H^{KI} mice were smaller, focal aggregations of cells distributed throughout the brain.

Collectively, our histopathology data demonstrate hyphal lesions early (day 1 P.I.) in both WT and CARD9-deficient mice, with accompanying early inflammatory responses in the WT brain and Y91H^{KI} brain more apparent. In serial evaluation of WT mouse brain, fungal lesions and peri-lesional inflammatory foci were no longer seen after day 1 P.I. In contrast, CARD9-deficient mouse brains demonstrated multinucleated giant cells and granulomatous lesions, similar to that seen in humans with CARD9 deficiency. Moreover, the inflammatory lesions appeared more numerous in *Card9*-/- mice than Y91H^{KI} mice (Figure 5).

Inflammatory monocytes accumulate early in the brain.

The identification of multinucleated giant cells and granulomata in this CARD9-deficient chronic invasive candidiasis mouse model, which mirrors what is seen in humans (1, 4, 22) (Figure 5), implicates a functional defect in monocytic responses. Thus, we used this model to define the monocyte responses in CARD9 deficiency. We characterized the early myeloid response in the brain by flow cytometry (Supplementary Figure 5). The number of Ly6C⁺ inflammatory monocytes increased by 35% in WT B6J mice at day 1 P.I. compared to PBS controls, while there was only a 14% increase in Card9-/- mice, however neither reached statistical significance (Figure 6A). In contrast, both WT B6N and Y91HKI mice had a significant increase (54% and 38% compared to PBS controls, respectively) in the number of inflammatory monocytes in the brain at day 1 P.I. (Figure 6B), consistent with our histopathology data showing cell aggregations at fungal lesions as early as day 1 on the B6N background (Supplementary Figure 3). In both CARD9-deficient mouse strains, there was an influx of Ly6C⁺ monocytes to the brain by day 4 P.I. that was not observed in WT mice (Figure 6A and B), coinciding with the divergence of brain fungal burden between CARD9-deficient (increasing) and WT mice (decreasing) (Figure 3C).

We next investigated the expression of surface markers on monocytes in the brain and found a significant increase in markers associated with activation, CD45 and MHCII, at day 1 P.I. on WT B6J cells, but not *Card9*-/- monocytes (Figure 6A and B). *Card9*-/- monocytes had increased levels of monocyte activation markers only at day 4 P.I., including CD45, CD11b, CD64, and MHCII. WT B6J monocytes remained activated at day 4 P.I., even as their absolute numbers began to decrease. While WT B6N monocytes only showed a trend toward activation,

Y91H^{KI} mice showed a significant increase in CD11b and CD64 expression, suggesting an active monocyte response by day 4 P.I. in this background as well.

As there were significantly higher monocyte numbers on the B6N background at day 1 P.I., but evidence of a higher activation status on monocytes in the WT B6J mice, we next investigated the number of Ly6C+MHCII+ monocyte-derived cells specifically, as this population is known to be essential for licensing neuroinflammatory responses in other models (23) (Figure 7). Indeed, both WT mouse strains had significantly higher MHCII+ monocyte-derived cells in the brain at day 1 P.I. compared to sham-infected control groups (Figure 7). Y91HKI mice also had increased MHCII+ monocyte-derived cells at day 1 P.I., while the number in *Card9*-/- mice was not significantly increased relative to sham control. These data support a role for activation and differentiation of Ly6C+ monocytes during the early responses to *Candida* in the brain and implicate the level of CARD9 functionality (intact in WT, hypomorphic in Y91HKI mice, and absent in the knock-out) in the regulation of these responses.

Microglia are the most abundant immune cell in the brain and are known to be important in anti-*Candida* resistance during infection in WT mice (11, 17). Thus, we next asked if microglia showed markers of activation, such as CD45, in CARD9-deficient mice. Microglia indeed showed increased CD45 at day 4 P.I. in both CARD9-deficient strains, but not WT mice, consistent with their activation during infection at this time point. Additionally, microglia on the WT B6J background showed an increase in cell number on day 1 P.I., which was not observed in the B6N background (Supplementary Figure 6, 7). Investigation of the activation of other mononuclear phagocytes, including Ly6C^{lo} monocytes, macrophages, and conventional dendritic cells (cDC) revealed signatures of activation by day 4 P.I., but no consistent pattern across the

different groups of mice (Supplementary Figure 6-8). There was no increase in eosinophils, NK cells, T cells, or B cells observed in any genotype up to day 4 P.I. (Supplementary Figure 8).

Collectively, these findings demonstrate a localized immune response in the brain of WT mice by day 4 P.I., characterized by the absence of the large influx of peripheral immune cells seen in high-dose models, particularly neutrophils. Moreover, they reveal an early mononuclear phagocyte response in the brain during CNS candidiasis that is dependent on CARD9 signaling. Specifically, the findings demonstrate the early recruitment and engagement of Ly6C⁺ monocytes, a process that is significantly delayed in CARD9 knock-out mice. Interestingly, despite this initial delay, the monocyte response in CARD9-deficient mice eventually becomes larger in scale compared to that observed in WT mice.

As early monocyte responses in the brain were demonstrated to be important in the high-dose model of candidiasis using $Ccr2^{-/-}$ mice, which lack circulating monocytes at steady state and show significant delays in monocyte egress from the bone marrow during infection (24), we assessed the importance of our observed monocyte response by evaluating $Ccr2^{-/-}$ mice infected with low dose C. albicans. Indeed, we show that by day 3 P.I., the percentage of $Ccr2^{-/-}$ mice with detectable fungal burden in the brain begins to diverge from WT controls (Supplementary Figure 9). By day 9 P.I., 71% of infected $Ccr2^{-/-}$ mice have detectable fungal burden, while only 33% of either WT genotypes do. Additionally, the median fungal burden in $Ccr2^{-/-}$ mice is 2 log-fold higher than the median of WT mice. These findings suggest that, in the setting of a CARD9-intact background, functional monocytic responses are important in mitigating CNS candidal disease.

To directly assess the role of the monocytic response observed in our chronic infection model, we used liposomal clodronate to deplete mononuclear phagocytes (Figure 8). WT mice of

both genotypes were able to clear the fungus from the brain and kidney when treated with liposome vehicle alone, but had detectable fungal burden in both tissues when treated with clodronate (Figure 8 and Supplementary Figure 9); this finding is consistent with that previously reported using clodronate-based depletion in a high-dose model (14) and confirms our Ccr2^{-/-} data on the importance of mononuclear phagocytes in this chronic invasive candidiasis model. CARD9-deficient mice did not clear the infection in the liposomal control treatment and showed fungal burden in both the brain and kidney. Y91HKI mice treated with clodronate showed higher candidal burden in both the brain and kidney, confirming that monocytes are necessary for antifungal immunity in the context of CARD9-deficiency in our low-dose model and suggesting that Y91HKI monocytes are at least partially protective, since their depletion leads to higher fungal burden. Card9^{-/-} mice treated with clodronate developed hypercoagulation resulting in 50% of mice not surviving to day 4 P.I. (Supplementary Figure 9C). Surviving mice showed only a small trend toward higher fungal burden in treated mice verses the liposomal control treatment (Supplementary Figure 9B), likely reflecting the existing delay of monocyte recruitment observed by flow cytometry.

Collectively, these findings demonstrate that monocytic responses are protective, as disruption of mononuclear phagocyte responses exacerbates disease outcomes in CARD9-deficient mice.

Impaired cellular responses of CARD9-deficient bone marrow-derived macrophages.

Bone marrow-derived cells from *Card9*^{-/-} mice have been used as a cellular model of CARD9-deficiency to show that CARD9 mediates specific anti-fungal effector functions, particularly the production of pro-inflammatory cytokines TNFA, IL6 and IL1B (4, 9, 25).

Monocytes derived from p.Y91H human patients have also demonstrated the importance of *Csf2* (Granulocyte-macrophage colony-stimulating factor, GM-CSF) production by these cells (3, 4). As our data suggest that the early responses of monocyte-derived cells in CARD9-deficiency are important in the context of CNS candidiasis, we infected BMDM with live *C. albicans* for 2 hours *in vitro* and investigated the proinflammatory cytokine response using qPCR (Figure 9A). Both CARD9-deficient genotypes showed impaired *Tnfa* production compared to WT controls. *Card9*-- BMDM produced *Csf2*, *Il1b*, and *Il6* at comparable levels to WT BMDM, however Y91H^{KI} BMDM showed significantly less production of these important inflammatory mediators.

Because CARD9 functions downstream of pattern recognition receptors (e.g. DECTIN-1) that have been shown to participate in phagocytosis of *C. albicans*, we next investigated whether the p.Y91H mutation affected internalization of yeast cells. Using live GFP-tagged *C. albicans* and the cell-impermeable dye Calcofluor White, internalized yeast were enumerated over the first hour of infection by confocal microscopy (Figure 9B). We found no difference in percent phagocytosis or phagocytic index between WT BMDM and both CARD9-deficient strains. This finding confirms previous studies showing that CARD9 is dispensable for phagocytosis of *C. albicans* in macrophages and demonstrates that p.Y91 is also not essential for internalization of yeast cells (9, 26).

As BMDM can directly kill internalized yeast cells, we tested the fungicidal activity of Y91H^{KI} BMDM to *C. albicans in vitro* using the XTT assay, a measure of cellular metabolism that reflects fungal viability (Figure 9C). CARD9-deficient BMDM, both *Card9*-/- and Y91H^{KI}, showed no defects in fungal killing when compared to WT controls. This data suggests that the

intrinsic capacity of these macrophages to kill phagocytosed yeast cells *in vitro* is not impaired by CARD9 deficiency.

Neutrophils respond to *C. albicans* in the brain in CARD9-deficiency.

High-dose models of disseminated candidiasis in *Card9*^{-/-} mice suggest that impaired neutrophil recruitment to the brain underlies disease (8, 9). Thus, we next investigated the neutrophil response in the brain during the early stages of chronic invasive candidiasis in our low-dose, CARD9-deficient mouse models (Figure 10). WT and CARD9-deficient mice do not recruit neutrophils at day 1 P.I., when we observed MHCII⁺ inflammatory monocytes increase in the brain, but CARD9-deficient mice have significantly higher neutrophil numbers at day 4 P.I. CARD9-deficient neutrophils consistently have higher CD11b expression than at day 1 P.I., suggesting they may be at a higher activation state (Figure 10A, B). WT mice do not show a significant increase in neutrophil cell numbers and do not have elevated expression of activation markers on neutrophils that are consistent between the WT strains.

Given the presence of neutrophils by day 4 P.I. in our CARD9-deficient mice, we next investigated neutrophil phagocytosis and neutrophil-mediated killing of *C. albicans*. Consistent with previous work evaluating CARD9-deficient human and mouse neutrophils (9, 27), *ex vivo Card9*-/- neutrophils showed no defect in phagocytosis or killing of serum-opsonized yeast cells, but did show impaired killing of non-opsonized yeast (Supplementary Figure 10). Neutrophils from the p.Y91H mouse phenocopied the *Card9*-/- neutrophils.

Our current mouse model revealed a neutrophil response to *C. albicans* in the brain following infection in CARD9-deficient mice. This finding stands in contrast to observations by others, who reported a limited or minimal neutrophil response (9). By immunohistochemistry on

a brain biopsy of a patient with the p.Y91H mutation, we confirm the modest and scattered presence of neutrophils *in situ* (Supplementary Figure 11). This suggests that our findings in mice do not inherently conflict with the human data and do not undermine the validity of this disease-recapitulating chronic candidiasis mouse model.

In sum, this data demonstrates there is some recruitment of neutrophils to the brain during the early stages of CNS candidiasis in the CARD9-deficient mouse, neutrophils are demonstrable in brain biopsy (reflecting later stages) of humans with CARD9-deficiency due to p.Y91H, and that *Card9*-/- and Y91H^{KI} neutrophils have comparable anti-candidal functions.

Discussion

Human CARD9 deficiency predisposes to invasive fungal infections in the absence of systemic disease, antibiotic or corticosteroid use, cancer, or trauma. The invasive candidiasis of CARD9 deficiency is most commonly caused by *C. albicans*, chronic in nature, late in disease onset, and has an unexplained predilection for the CNS. Understanding the immunologic basis by which loss of CARD9 function leads to such a unique syndrome has been hampered by the lack of experimental models that recapitulate these key features.

Here, we first generated mice homozygous for the recurring p.Y91H human mutation. Using a standard high-dose model of candidemia, the Y91H^{KI} mouse phenocopies the Card9^{-/-} mouse with respect to acuity, morbidity, mortality, and tissue fungal burden, relative to WT mice. Interestingly, Card9^{-/-} mice die slightly earlier than Y91H^{KI} mice, which may be related to the hypomorphic nature of the latter. Altogether, these findings confirm the utility of the Y91HKI mouse to better understand the antifungal role of CARD9. However, the fulminant and disseminated nature of fungal disease with this high-dose strategy does not accurately recapitulate human CARD9 deficiency. By titrating the candidal dose to the CARD9 genotype, we established a model in which mutant mice demonstrate chronicity of infection, overt neurological symptoms with CNS predilection, and histopathological multi-nucleated giant cells/granulomata surrounding fungal lesions; these features were elicited at an LD₅₀ dose that was at least 2-log₁₀ fold lower than the standard, high-dose method. At this lower dose, WT mice completely resolved this infection, displaying no morbidity or mortality. In fact, in our approach, skull destruction is uniquely seen in Card9^{-/-} mice, consistent with the original report on CARD9 deficiency (28), but not observed in the Y91HKI mouse in the time frame of these experiments, also mirroring what is observed clinically (3, 4). These aggregated features, which are more

aligned with the distinctive clinical features of the human syndrome and are not observed in the high-dose strategy, supports the relevance of this mouse model to define the fungal immunopathophysiology of CARD9 deficiency. It also provides a framework for future antifungal studies of other CARD9 mutations.

We then used this CARD9-mutant, chronic invasive candidiasis model to begin to decipher the immunopathology of CNS candidiasis. Because of previous work demonstrating impaired monocyte and neutrophil responses in humans (3, 4, 9, 27), and our findings of granulomata in CARD9-deficient mice and humans, we focused on early myeloid responses. Our results demonstrate CARD9 knock-out mice have a delay in the accumulation of activated Ly6C⁺MHCII⁺ monocytes in their brain early in infection, but both CARD9-deficient mice have an abnormal accumulation of these cells by day 4 P.I., corresponding to an increased brain fungal burden histologically, preceding their typical clinical end-point starting at ~day 9. Ly6C⁺ monocytes in the brain that upregulate MHCII can license neuroinflammation in models of sterile inflammatory disorders, such as EAE, a mouse model of multiple sclerosis (23). The increase in Ly6C⁺ MHCII⁺ monocyte-derived cells in the brain of infected WT mice is observed at day 1 P.I., implicating this cell type among the earliest responses to candidal brain invasion. These data suggest that CARD9 may be essential for the recruitment or functional differentiation of Ly6C⁺ monocytes in the infected brain, a response that preceded neutrophil influx as fungal burden began to increase in CARD9-deficient mice. Our results are consistent with the observations of Wu et al. showing WT mice that developed transient cerebritis after C. albicans challenge relied on microglia, in the presence of monocytes but not neutrophils, to clear the fungus (17). We have therefore identified an early, asymptomatic window of time in the

pathogenesis of CNS candidiasis associated with a CARD9-dependent activation and influx of Ly6C⁺ monocytes.

The abnormal recruitment of monocytes observed, along with histopathological evidence of multinucleated giant cells/granulomata, may reflect a mechanism for fungal control; on the other hand, they may also be deleterious and cause immunopathology. To distinguish between these two possibilities, we showed, through the use of a *Ccr2*-/- mouse (which lack circulating Ly6C+ monocytes (24) but are CARD9-intact), that these mice could not clear the fungus from their brains over the course of infection, supporting the premise that influx of Ly6C+ monocytes are protective for CNS candidiasis. We complemented this evaluation with clodronate-based monocyte depletion experiments in our CARD9-mutant mice, demonstrating that their loss of this response enhanced fungal growth. Collectively, these findings support an important role for mononuclear phagocytes in mitigating CNS candidiasis and show that the abnormal monocytic response observed in the CARD9-deficient mice are at least partially functional, and protective. That these monocytic responses are ultimately unable to control candidal growth may underlie the chronic nature of their CNS infection.

While Y91H^{KI} mice can recruit monocytes in the brain at the same level as WT mice, and our clodronate data confirm their protective nature, our *in vitro* data using BMDM as a model of terminally-differentiated monocytes support the premise that some functions of specialized monocytic cells remain functionally impaired. Our BMDM-mediated phagocytosis experiments revealed no differences between genotypes. Likewise, assessment of BMDM-mediated killing of candidal yeast cells exposed no differences. Because impaired pro-inflammatory cytokine responses, including IL1B, IL6, TNFA, and GM-CSF, to *C. albicans* and fungal agonists is a consistent cellular phenotype of CARD9 loss-of-function in human monocytes (4, 9, 27), we

evaluated these in our murine BMDM: Both CARD9-deficient genotypes showed impaired *Tnfa* responses, but only Y91HKI BMDM also showed impairment in Il1b, Il6, and Csf2 production. The stochastic distribution of infected foci in the brain precluded assessing these functions in situ, so it remains unclear whether these impaired responses occur in vivo within monocytic, macrophagic, and/or microglial cells. As TNFa is important for granuloma integrity (17, 29, 30), the impaired TNFa responses shared by CARD9-mutant BMDM may account for the development of multinucleated giant cells/granuloma-like lesions that may not be able to ultimately contain C. albicans. Clearly, a broader array of cytokine responses, including spatial assessment and additional CNS cells, is needed to better understand this pathology. Nonetheless, we demonstrate for the first time to our knowledge that, when challenged with a given C. albicans strain, CARD9-deficient mice of different genotypes (null vs. hypomorphic p.Y91H) not only have differences in severity of manifestations at the organismal level, but that the immune response and cellular impairments of each may also be subtly distinct. Whether there are differences in immunological response to C. albicans between distinct CARD9 hypomorphic mutations (for example, based on protein location) is speculative, but may help clarify variations in clinical trajectory among CARD9-deficient patients. Moreover, functional differences between CARD9 genotypes, alone or perhaps in conjunction with functional variants in other genes, may account for the enigmatic susceptibility to the other but seemingly-ubiquitous fungi seen in various CARD9-deficient patients.

Interestingly, our mouse model shows that the Y91H^{KI} BMDM have impaired *Csf2* (GM-CSF) responses compared to WT counterparts, which was not seen in *Card9*-/- mice. It remains uncertain whether this finding indicates that different CARD9 mutations have distinct effects on GM-CSF responses, perhaps accounting for the observed divergent clinical responses to adjunct

GM-CSF therapy between patients with *C. albicans* CNS infection (3, 4, 9). Alternatively, other factors may be at play: For example, in the two patients we reported where it was beneficial, GM-CSF was given after surgical resection (which debulks the fungal burden), whereas in the patient where it did not provide benefit, no surgical resection was performed (3, 4, 31). Thus, it may be that debulking of brain lesions is necessary for GM-CSF to exert a beneficial effect (e.g. by enabling the more feasible neutralization of any newly developing infectious focus).

Alternatively, it may suggest that the beneficial effect of GM-CSF therapy is exerted outside of the brain. Indeed, with the establishment of this pathogenetically-relevant model, we can now specifically address this question, as well as interrogate the impact of different candidal species, different routes of infection, and responses to different fungal genera altogether.

Another enigmatic feature of CNS candidiasis of CARD9-deficiency is the aberrant neutrophil response. Drummond *et al.* have shown that neutrophil numbers are unexpectedly low, but definitely not absent, in human CARD9-deficiency; that the neutrophil recruitment response in the mouse brain is proportional to the fungal burden in WT mice but insufficient in CARD9-deficient mice when both genotypes have high brain burden; and that *Card9*-/- neutrophils have impaired *Candida* killing against the unopsonized yeast form of the fungus (9). The influx of neutrophils in our CARD9-mutant mice at day 4 P.I. prompted us to re-evaluate patient samples, where neutrophils were also seen (although they were not the predominant component of the inflammatory response). The discrepancy in the extent of neutrophil response between the CARD9-deficient mice and in patients could be attributed to differences in the timing of sampling, as onset of infection is precisely known in mice, allowing for early sampling, while patient samples are by definition collected later, during symptomatic stages of the disease. The neutrophils from *Card9*-/- or Y91H^{KI} had similar functional capacity, namely, intact

phagocytosis of both opsonized and unopsonized yeast cells, intact killing of opsonized yeast, and impaired killing of unopsonized yeast, similar to what has been previously shown (9, 27). We could detect no differences in the patterns of neutrophil recruitment or dysfunction between the knock-out and the Y91H mutant suggesting that neutrophil dysfunction is unlikely to explain differences in disease severity seen between the two CARD9 mutants. Furthermore, eosinophilic infiltration of CNS tissue can be seen in some patients with CARD9 deficiency, as it can in other patients who do not have CARD9 deficiency but who have chronic fungal infections, and indeed three of the Y91H^{KI} mice analyzed for flow cytometry showed eosinophil recruitment to the brain by day 4 P.I. (Supplementary Figure 8). Sampling in our model may have been too early in disease to fully appreciate eosinophilic responses during chronic fungal infection. Overall, these findings support a general concept that loss of CARD9 function alters neutrophil recruitment into the CNS space following *C. albicans* infection. Further investigation into the kinetics of the neutrophil response in this chronic candidiasis mouse model will help determine how closely it mirrors the human condition.

In summary, by tailoring the fungal challenge to the susceptibility gene, we have established a mouse model of CARD9 deficiency that more-accurately recapitulates the human inborn error of immunity at the clinical and histopathological levels, enabling investigations into the immunopathogenesis underlying chronic CNS candidiasis. Our model identifies that loss of CARD9 function associates with impaired tissue control of low fungal burden and cerebral multinucleated giant cells/granulomata, coupled with abnormal influx of Ly6C⁺ monocytederived cells and defective BMDM responses, ultimately contributing to indolent infection with late disease. With this approach, we have additionally shown that p.Y91H is indeed detrimental, but results in subtle immunologic differences compared to its null counterpart, raising the

possibility that different mutations impact CARD9's loss of function in distinct and consequential ways. More broadly, our experimentally established framework provides a necessary tool to not only pinpoint how loss of CARD9 function mediates fungal disease, but also for the development of mechanism-targeting therapeutic interventions.

Materials and Methods

Mice. C57BL/6J, *Card9*^{-/-}, C57BL/6N, and Y91H^{KI} mice were age and sex matched within each experiment. Results from male mice aged 7-12 weeks are shown for fungal burden experiments. All other experiments show female mice aged 7-12 weeks unless otherwise specified. C57BL/6J, *Card9*^{-/-}, and *Ccr2*^{-/-} mice were purchased from Jackson Laboratories. C57BL/6N were purchased from Envigo. Y91H^{KI} mice were generated by CRISPR-Cas9 at McGill Integrated Core for Animal Modeling (MICAM) by microinjecting a gRNA (TCTACTACCCTCAGTTATAC) with a ssODN

TCTACTACCCTCAGTTACACCGCAAAGTCACTGGCAAGGAGCCAGCACGCGTCTTCT CCATGATCATTGgtgagaggcacgggt) which were both purchased from IDT. The gRNA was complexed with the protein Cas9 and microinjected into the pronucleus of the C57BL/6N embryo with the ssODN. These embryos were then transferred into pseudo-pregnant CD-1 females to generate potential F0 mice. After pups were born, ear biopsies were taken to screen for the p.Y91H mutation and a founder male was identified and named Card9em2Sq. The male founder was outcrossed to wild-type C57BL/6N females and heterozygous Card9em2Sq F1 mice were subsequently intercrossed to generate homozygous Card9em2Sq mice (Y91HKI). All animals were maintained in compliance with the Canadian Council on Animal Care and all experiments were approved by the McGill University animal care and use committee. All mice were backcrossed to their respective wild-type strains every 3-4 generations.

Sex as a biological variable. Experimental findings were confirmed in both sexes. Sex matching within each experiment decreased total statistical variation, and no significant differences

between male and female mice were detected for any of the parameters measured. For human samples, sex was not analyzed as a biological variable in this study. Patients were evaluated based on clinical referral patterns, and the potential relevance of sex differences in CARD9-deficient candidiasis remains unknown.

Candida albicans. C. albicans strain SC5314 was used for all experiments, unless otherwise noted. GFP tagged C. albicans (gift from Robert T. Wheeler; Department of Molecular & Biomedical Sciences, University of Maine, Orono, Maine, USA) (32) was used for the phagocytosis assays. Both strains of C. albicans were propagated on Sabouraud Glucose Agar (SGA) plates containing chloramphenicol (Sigma). Single colonies were subcultured overnight in liquid yeast peptone dextrose (YPD) media (Sigma) at 30°C in a shaking incubator. 1mL of culture was washed three times in PBS (Wisent), then fungal cells counted by hemocytometer and the sole presence of yeast cells confirmed by brightfield microscopy. Washed C. albicans yeast were diluted to the appropriate concentration per experiment in BMDM media. Dilutions were confirmed by quantitative culture on SGA plates incubated at 30°C for 48hr.

Intravenous injection. Washed and diluted *C. albicans* yeast from overnight culture were prepared in PBS at the concentration indicated for each experiment. Mice were heated under a red lamp for 4min per cage, then 100µl per mouse of *C. albicans* in PBS, or PBS alone, was injected via lateral tail vein. Mice were monitored immediately after injection until normal grooming resumed.

Fungal Burden. At each time point P.I. mice were euthanized by treatment with isoflurane followed by CO₂ according to the ethical guidelines of the animal resource department of the McGill University Health Centre. Tissues were aseptically removed, weighed, and placed in 1mL PBS on ice. All tissue was mechanically homogenized, then serially diluted in PBS.

Dilutions were plated in duplicate on Sabouraud agar plates containing chloramphenicol, incubated at 30°C for 48hr, then CFU enumerated. CFU below detection (zero CFU) are listed as "1" when graphed in log-scale.

Histopathology. Mice were perfused with 20mL of 10% formalin by intracardiac puncture. Tissues were stored in 10% formalin, then embedded in parafilm, sectioned, and stained with Periodic acid–Schiff (PAS) stain, hematoxylin and eosin (H&E) stain, or Grocott-Gomori's methenamine silver (GMS) stain. Images were obtained by Aperio AT Turbo digital slide scanner using a 20x objective, and close-ups with a brightfield microscope using a 40x objective. Human p.Y91H patient biopsies were stained either with H&E or immunohistochemistry was performed with neutrophil elastase antibody (Abcam, clone ERP7479), dilution 1/1000, pretreatment with CC1 on a Ventana Discovery instrument. Human H&E stained samples were imaged with 400x magnification using a BX53 Olympus microscope and DP21 Olympus digital camera.

Survival and observation of mouse behaviour. Mice were weighed and original weight recorded, then mice observed for baseline bright, alert, and responsive behaviour. Mice were injected with *C. albicans* by lateral tail vein in the amount listed for each experiment. Mice were weighed daily and monitored for signs of morbidity including piloerection, hunching, squinting, and lethargy throughout the 30-day experiment. Endpoint criteria were loss of 20% original weight, or three or more signs of morbidity combined with lethargy. Mice that displayed symptoms such as shaking, head tilting, altered gait, or unidirectional walking but were alert and responsive without weight loss were monitored twice daily. Videos of mouse behaviour and images of anatomy were taken with an iPhone SE 12-megapixel camera.

Bone marrow derived macrophages (BMDM). Whole bone marrow from 2 femurs was aseptically isolated in 1mL PBS. 10µl of the single cell suspension was treated with ammonium-chloride-potassium (ACK) lysis solution to lyse red blood cells and washed in PBS. Live cells from this sample were identified by 4% trypan blue exclusion and counted by hemocytometer under a brightfield microscope. Eight million bone marrow cells were added to 10cm sterile petri dishes containing 10mL of BMDM media and 100ng/mL of M-CSF (Peprotech). After 3 days, 4mL of BMDM media and 50ng/mL of M-CSF were added to cultures. BMDM were seeded for experiments after 6 days in culture. BMDM media was RPMI-1640 (Wisent) supplemented with 10% fetal bovine serum (FBS, Wisent), 10mM HEPES (Wisent), 1mM sodium pyruvate (Wisent), 1% essential and non-essential amino acids (Wisent) and 100U/ml penicillin/streptomycin (Wisent) and pH balanced with 5N NaOH.

BMDM *In vitro* Infection. BMDM from mice of each genotype were seeded into 6-well plates at 1million cells per well and allowed to adhere overnight (16~20 hours). *C. albicans* were prepared as for *in vivo* infection. BMDM were challenged with live *C. albicans* at an MOI 1 in BMDM media for 2 hours followed by RNA extraction. BMDM pulsed with *C. albicans* but immediately washed with PBS and RNA extracted were used as corresponding sham-treatment controls.

RT-PCR. RNA from BMDM was extracted using TRIZOL Reagent (Invitrogen) according to manufacturer's instructions. 500 ng of RNA was reverse transcribed using the Maxima H Minus First Strand cDNA Synthesis Kit (Thermo Fisher Scientific). PCR for *Card9* cDNA was done using Phusion High-Fidelity DNA Polymerase (Thermo Fisher Scientific) according to the manufacturer's instructions.

qPCR. TaqMan Gene Expression Assays were conducted on an Applied Biosystems 7300 Real-Time PCR System using TaqMan Fast Advanced Master Mix (Applied Biosystems, cat# 4444554) according to manufacturer's instructions for detection of *Il6* (Mm00446190_m1), *Il1b* (Mm01336189_m1), *Csf2* (Mm00438328_m1) and *Tnfa* (Mm00443258_m1). Targeted genes were normalized with reference genes *B2m* (Mm00437762_m1) and beta-actin (Mm02619580_g1). The differences between samples were calculated using the ΔΔCT method. Fold-change is reported relative to levels observed in sham-treated BMDM. BMDM derived from 12 mice per genotype were used.

BMDM Phagocytosis Assay. After 6 days in culture, BMDM were seeded into 24-well plates containing a round micro cover glass (Electron Microscopy Sciences, US. Cat#72230-01) in each well, at 0.3 million cells per well and allowed to adhere overnight (16 \sim 20 hours). GFP tagged C. albicans were prepared as for in vivo infection. BMDM were challenged with live C. albicans at an MOI 1 and 0.1 for 15, 30 and 60 minutes and then fixed with 2% Paraformaldehyde in PBS for 10 minutes (Thermo Fisher Scientific Cat# J19943-K2). To distinguish between intracellular and extracellular C. albicans, extracellular yeast were differentially stained with Calcofluor White (Sigma-Aldrich, Cat#18909-100ml-F) for 10 minutes and washed with PBS. BMDM pulsed with C. albicans but immediately fixed with 2% Paraformaldehyde were used as 0-minute baseline controls. Samples were air dried and mounted on precleaned microscope slides (Fisher Scientific, Cat# 12-550-15) using IMM mounting medium (Ibidi, Germany, Cat#50001). Imaging was done with an Echo 4-in-one fluorescence microscope (Discover Echo Inc. model: RVL2-K2). Images were obtained using a 20 X objective lens and a minimum of five random fields were analyzed for each sample. Cell counting was performed manually with open resource Fiji software (ImageJ 1.53t). Percent Phagocytosis was calculated as follows: % Phagocytosis =

Phagocytic Index (PI) was calculated as follows: Phagocytic index = (total number of engulfed C. albicans / total number of counted BMDM) × (number of BMDM containing engulfed C. albicans / total number of counted BMDM) × 100. Data from 9 mice per genotype were pooled for analysis.

2,3-Bis-(2-Methoxy-4-Nitro-Sulfophenyl)-2 (XTT) Assay. BMDM were plated at $9x10^5$ cells per well in 12-well plates. The next day, cells were infected with $9x10^4$ live *C. albicans* (MOI 0.1), centrifuged 3 min at 800 g and incubated at 37° C for 6 hours. BMDM lysis was achieved using a 0.1% Triton X-100 solution, and the remaining yeast were incubated in PBS containing $500 \mu \text{g/ml}$ XTT (X6493, Invitrogen) and $50 \mu \text{g/ml}$ Coenzyme Q0 (20504, Cayman Chemical) for 2 hours at 37° C. DMSO was then added to each well before recuperating and centrifuging the solution at 15,493 g for 5 min. Absorbance was measured at 450 nm and 650 nm using a microplate reader, and the net absorbance (450 nm-650 nm) was used for analysis.

Western blot. Protein from BMDM was isolated using RIPA buffer (Thermo Fisher Scientific) containing cOmplete Mini Protease Inhibitor Cocktail (Roche) and PhosSTOP (Roche), then boiled in Blot Sample Reducing Agent (Thermo Fisher Scientific) and sample buffer (Novex). Protein was separated by SDS-PAGE on premade gels (Novex) before transfer to membrane via iBlot Gel Transfer Device (Invitrogen). Membrane was blocked in 10% skim milk in TBST then blotted using rabbit anti-CARD9 polyclonal antibody (Abnova, catalog #PAB12874) and mouse anti-GAPDH antibody (Millipore, catalog #MAB374) overnight at 4°C shaking. Membrane was washed in TBST then blotted with secondary antibodies: Goat anti-Rabbit IgG DyLight 800 (Invitrogen, catalog #SA5-35571) and Goat anti-Mouse IgG DyLight 680 (Invitrogen, catalog #35518) for 1hr at room temperature, shaking. Membrane was washed in TBST, then PBS and

imaged on an Odyssey Infrared Imager (v3.0, LI-COR) using Odyssey Application Software (LI-COR).

Sanger Sequencing. The exon 3 of the CARD9 gene was PCR amplified from genomic DNA using primers designed to flank c.T271. Sequencing was performed at the McGill University and Génome Québec Innovation Centre. Sequencing analyses were performed on Sequencher sequence analysis software (Gene Codes Corporation).

CT-scan of mouse skull. Scan was done with a nanoScan SPECT/CT (Mediso USA), at 35 kVp X-ray source voltage 980 µA current, 450 ms exposure time, and scan method semicircular. The tomographic reconstruction of the projections resulted in 1075 slices with isotropic 20 µm voxel size.

Single cell suspensions. For brain, spleen, and kidney, mice were ethically euthanized then perfused with 30mL PBS by intracardiac puncture. Whole tissue was aseptically harvested, weighed, minced in minimal PBS, and placed in 1x HBSS (Wisent) containing collagenase D (Sigma) and DNase I (Sigma) on ice. Tissue was digested at 37 °C for 30min in a shaking incubator (200rpm), then passed through a 100micron cell strainer into a total volume of 17mL 1x HBSS. After centrifugation, cells were brought up in 10mL of 37% Percoll (GE Healthcare) in HBSS and spun at 500g for 10min and allowed to come to a stop with no brake. Myelin (brain) and debris (kidney, spleen) was removed by vacuum and cells washed in 5mL 1x HBSS. After red blood cell lysis in ACK, single cell suspensions were resuspended in 200μl FACS buffer (0.5% BSA in PBS, Sigma) for enumeration. Live cells were identified by 4% trypan blue exclusion and counted by hemocytometer under a brightfield microscope. For bone marrow: both femurs were aseptically removed, and the ends cut to isolate the femoral shaft. Bone marrow was isolated by centrifugation into 200μL RPMI media, the volume of both femurs combined, and

the total volume increased to 1mL RPMI. Live cells were identified by 4% trypan blue exclusion and counted by hemocytometer under a brightfield microscope. 1million cells per mouse were then treated with ACK for red blood cell lysis and stained for flow cytometry. For blood: Blood was collected by cardiac puncture into heparin coated tubes (BD Microtainer tubes with lithium heparin). 25 μ L of blood was directly stained for flow cytometry, then brought up in ACK for red blood cell lysis and washed with FACS buffer. Stained blood samples were then fixed in 1% PFA.

Flow cytometry. Single cell suspensions were stained with viability dye eFluor 506 (Invitrogen catalog #50-246-097; 20 min; 4 °C) and surface blocked with anti-CD16/32 (BD Biosciences, clone 93) in 0.5% BSA/PBS solution to block non-specific antibody interaction with Fc receptors (10 min; 4 °C). Cells were then surface stained with anti-CD45.2 in BV421 (eBioscience, clone 104), anti-CD11b in PE-Cy7 (BD Bioscience, clone M1/7), anti-Ly6G in Alexa700 (Biolegend, clone 1A8), anti-Ly6C in APC (Biolegend, clone AL-21), anti-CD11c in PerCP Cy5.5 (eBioscience, clone N418), anti-CX₃CR1 in BV650 (Biolegend, clone SA011F11), anti-CD3 in PE (Biolegend, clone 145-2C11), anti-CD19 in BV786 (BD Bioscience, clone 1D3), anti-MHCII in BV605 (BD Bioscience, clone M5/114.15.2), anti-NK1.1 in APC-780 (Invitrogen, clone PK136), anti-SiglecF in PE-CF594 (BD Horizon, clone E50-2440), anti-CD64 in FITC (Biolegend, clone X54-5/7.1), and control samples with FMO antibody cocktails, for 30min at 4 °C. Cells were washed once in FACS buffer, then fixed in 1% PFA (Alfa Aesar) in PBS. Flow cytometry was performed using BD LSRFortessa X-20 (BD Biosciences) with FACSDiva Software version 8.0.1 (BD Biosciences). Analysis was performed using FlowJo software version 10.4.2. For blood processing in the clodronate experiments, see below.

Bone marrow derived neutrophils. Whole bone marrow was flushed from 2 femurs and 2 tibias using RPMI 1640 (Wisent) supplemented with 10% fetal bovine serum (FBS, Wisent) and 2mM EDTA (Wisent). Cell suspension was filtered on a 100 mm filter and cells were counted by hemocytometer under a brightfield microscope. Neutrophils were purified by negative magnetic bead selection using MojoSort Mouse Neutrophil Isolation Kit (BioLegend) according to the manufacturer's instructions. Bone marrow-enriched neutrophils (CD45+CD11b+Ly-6G+) had > 80% purity and > 90% viability as determined by flow cytometry using BD FACSCanto II cytometer (BD Biosciences).

Neutrophil killing assay. Neutrophil killing of *Candida albicans* was determined by CFU enumeration. Bone marrow-enriched neutrophils were seeded into 48-well plates at 0.25 million cells per well and allowed to settle for 30 minutes at 37°C, 5% CO₂ while GFP tagged *C. albicans* was opsonized with 10% fresh mouse serum in 1X HBSS for 30 minutes at 4°C. Unopsonized or serum-opsonized *C. albicans* were added to neutrophils at an MOI 0.05 for 3 hours and then cells were lysed with 0.02% Triton X-100 in ice-cold water for 5 minutes and plated. Neutrophil killing was calculated as the (CFU from wells with neutrophils) / (CFU from control wells without neutrophils) x100%.

Neutrophil phagocytosis Assay. A total of 0.5 million bone marrow-enriched neutrophils were incubated with unopsonized or mouse serum-opsonized GFP tagged *C. albicans* at an MOI 0.5 in a 2 ml round-bottom tube for 30 minutes on a revolver rotator end-to-tail at 37°C, 5% CO₂. Infected neutrophils were then stained with 1:500 anti-Ly-6G in APC (BioLegend, clone 1A8) in PBS with 1:100 anti-CD16/CD32 Fc block (BD Biosciences, clone 93) for 30 min at 4°C. To distinguish between intracellular and extracellular *C. albicans*, extracellular yeasts were differentially stained with Uvitex 2B (Polysciences) in PBS for 1 min at RT and washed with

PBS then fixed with 1% PFA (Alfa Aesar). Samples were analyzed on the Amnis ImageStream^X Mk II imaging flow cytometer with INSPIRE software (Cytek Biosciences) at the RI-MUHC Immunophenotyping core platform. Data analysis was done using the IDEAS v6.2 software (Cytek Biosciences). The neutrophils associated with C. albicans (this population includes neutrophils with both internalized and neutrophil-bound yeasts) is shown as a percentage of GFP⁺Ly-6G⁺ neutrophils. Percent of neutrophils with internalized C. albicans is the percentage of gated Uvitex-GFP+Ly-6G+ neutrophils. The number of yeasts per neutrophil was calculated using the Spot Count Wizard to create a GFP spot count feature in the Uvitex GFP+Ly-6G+ gate. Clodronate cell depletion. Mice were injected i.p. with 200 ml of clodronate or control liposomes (Encapsula Nano Sciences) 24h and 1h prior C. albicans i.v. infection, as well as 24h and 72h post-infection (4 injections total). At day 4 post-infection, kidneys and brain were aseptically removed, and fungal burden was assessed as described above. For analysis of the blood by flow cytometry, blood was collected by cardiac puncture into heparin coated tubes (BD Microtainer tubes with lithium heparin). 50 µL of blood was directly surface blocked with anti-CD16/32 (BD Biosciences, clone 93) and stained with anti-CD45.2 in BV421 (eBioscience, clone 104), anti-CD11b in PE (eBioscience, clone M1/7), anti-Ly6G in APC (Biolegend, clone A18) and anti-CD115 in PerCP-eF710 (eBioscience, clone AFS98), for 30min at 4 °C. Red blood cell lysis was performed with BD FACS Lysis Solution (BD Biosciences) for 10 min at room temperature. Cells were washed once in FACS buffer, then fixed in 1% PFA (Alfa Aesar) in PBS. Flow cytometry was performed using BD FACSCanto II cytometer (BD Biosciences) with FACSDiva Software version 8.0.1 (BD Biosciences). Analysis was performed using FlowJo software version 10.4.2.

Primers. Primers are listed in the 5' to 3' direction. Fwd: Forward primer. Rev: Reverse primer.

Card9 Exon 3 Amplification Fwd: GCAGGGCGCCTTATTCAATG; Rev:

GGCTCCCCTTCTAGAGACCA.

c.T271C Sequencing Primers Fwd: CATCTCCAAGAGCCTCCACC; Rev:

TCATAGAAGCCAGGACCCGA.

Card9 cDNA (RT-PCR) Fwd: CTCACTGCCTCAGGATCTGG; Rev:

CCCTGTCTGCCAGTACACCT.

<u>Card9-/-</u> genotyping (Jackson Laboratories) Common: CTGACAGGGAACAGAAGGTG; WT:

AGGACTTTGCACTGGCGTAG; KO:TGCCTGCTTGCCGAATATC.

Statistics. Statistical analysis was performed using GraphPad Prism 8.0.2(263) software. Unless otherwise specified, one-way analysis of variance followed by a multiple comparison test (Tukey's) was used to test differences between groups. Kruskal–Wallis was used for nonparametric data (qPCR and phagocytosis assay), Two-way analysis of variance was used for grouped data, followed by a multiple comparison test (Sidak). P-value < 0.05 was considered significant.

Study Approval. The mouse study was conducted under the RI-MUHC–approved animal use protocol 7829 (Animal Care Committee of McGill University). The human study was reviewed and approved by the MUHC Research Ethics Board (REB), Montréal, Québec, Canada (protocol GEN10-256). All patients provided informed consent prior to their participation in the study.

Data and materials availability. Values for all data points in graphs can be found in the Supplemental Supporting Data Values file.

Contribution of Authors:

DCV, MD, ML conceptualized the project. ML performed all animal infections and experiments, and downstream analysis. ML created and assembled all figures. IA, ABe, and SQ generated the Y91H^{KI} mice and assisted with breeding. IA performed *ex vivo* neutrophil experiments and, together with ABe, performed the clodronate experiments. AB assisted with fungal burden experiments and animal harvests. MAD performed the XTT assay. YL performed the phagocytosis and qPCR experiments in BMDM. LR assisted with fungal burden experiments and provided helpful discussions. WBZ assisted with fungal burden experiments. CG assisted with animal harvests. JL helped prepare the figures. SB, MKB, YS, BS, and MSL provided helpful discussions and experimental support. MCG provided human histopathology data. RTW provided the *C. albicans* and technical support. ML, MD and DCV drafted and edited the manuscript. DCV and MD supervised the project.

Acknowledgements

The authors would like to thank the Small Animal Imaging Labs (SAIL) Platform and the Histopathology Platform at the McGill University Health Centre Research Institute (RI-MUHC) for their help with the CT-scan and histopathology staining, respectively. This work was supported by Canadian Institutes of Health Research (CIHR; grant: 201809PJT-407084-IT-CFAC-163753), the Rare Diseases: Models & Mechanisms network (RDMM) grant (RCN-137793), and Fonds de recherche du Québec – Santé (FRQS) clinician-scientist Junior 2 scholar

award to DCV and scientist senior scholar award to MD. DCV has received clinical trial support from: Cidara Therapuetics; CSL Behring; and Janssen Pharmaceuticals. DCV has served on advisory boards for: CSL Behring; Novartis Canada; and UCB Biosciences GmbH. DCV has received speaker honoraria from: CSL Behring; Merck Canada. DCV has a patent application pending (Electronic Filing System ID: 40101099) unrelated to this work.

References

- 1. Gavino C, Landekic M, and Vinh DC. In: MacKay I, and Rose NR eds. *Encyclopedia of Medical Immunology: Immunodeficiency Diseases*. New York, NY: Springer New York; 2017:1-22.
- 2. Vaezi A, Fakhim H, Abtahian Z, et al. Frequency and Geographic Distribution of CARD9 Mutations in Patients With Severe Fungal Infections. *Front Microbiol*. 2018;9:2434.
- 3. Gavino C, Hamel N, Zeng JB, et al. Impaired RASGRF1/ERK-mediated GM-CSF response characterizes CARD9 deficiency in French-Canadians. *J Allergy Clin Immunol*. 2016;137(4):1178-88.e7.
- 4. Gavino C, Cotter A, Lichtenstein D, et al. CARD9 deficiency and spontaneous central nervous system candidiasis: complete clinical remission with GM-CSF therapy. *Clin Infect Dis.* 2014;59(1):81-4.
- 5. Kennedy MJ, and Volz PA. Effect of various antibiotics on gastrointestinal colonization and dissemination by Candida albicans. *Sabouraudia*. 1985;23(4):265-73.
- 6. Koh AY, Köhler JR, Coggshall KT, et al. Mucosal damage and neutropenia are required for Candida albicans dissemination. *PLoS Pathog.* 2008;4(2):e35.
- 7. Koh AY. Murine models of Candida gastrointestinal colonization and dissemination. *Eukaryot Cell.* 2013;12(11):1416-22.
- 8. Drummond RA, Swamydas M, Oikonomou V, et al. CARD9+ microglia promote antifungal immunity via IL-1β- and CXCL1-mediated neutrophil recruitment. *Nature Immunology*. 2019;20(5):559-70.
- 9. Drummond RA, Collar AL, Swamydas M, et al. CARD9-Dependent Neutrophil Recruitment Protects against Fungal Invasion of the Central Nervous System. *PLOS Pathogens*. 2015;11(12):e1005293.
- 10. Spellberg B, Ibrahim AS, Edwards JE, Jr., et al. Mice with Disseminated Candidiasis Die of Progressive Sepsis. *The Journal of Infectious Diseases*. 2005;192(2):336-43.
- 11. Lionakis MS, Lim JK, Lee CC, et al. Organ-specific innate immune responses in a mouse model of invasive candidiasis. *J Innate Immun*. 2011;3(2):180-99.
- 12. Lionakis MS, Fischer BG, Lim JK, et al. Chemokine receptor Ccr1 drives neutrophil-mediated kidney immunopathology and mortality in invasive candidiasis. *PLoS Pathog*. 2012;8(8):e1002865.
- 13. MacCallum DM, Castillo L, Brown AJP, et al. Early-expressed chemokines predict kidney immunopathology in experimental disseminated Candida albicans infections. *PLoS One.* 2009;4(7):e6420-e.
- 14. Qian Q, Jutila MA, Van Rooijen N, et al. Elimination of mouse splenic macrophages correlates with increased susceptibility to experimental disseminated candidiasis. *J Immunol.* 1994;152(10):5000-8.
- 15. Domínguez-Andrés J, Feo-Lucas L, Minguito de la Escalera M, et al. Inflammatory Ly6Chigh Monocytes Protect against Candidiasis through IL-15-Driven NK Cell/Neutrophil Activation. *Immunity*. 2017;46(6):1059-72.e4.
- 16. Corvilain E, Casanova J-L, and Puel A. Inherited CARD9 Deficiency: Invasive Disease Caused by Ascomycete Fungi in Previously Healthy Children and Adults. *J Clin Immunol*. 2018;38(6):656-93.

- 17. Wu Y, Du S, Johnson JL, et al. Microglia and amyloid precursor protein coordinate control of transient Candida cerebritis with memory deficits. *Nature Communications*. 2019;10(1):58.
- 18. Lanternier F, Mahdaviani SA, Barbati E, et al. Inherited CARD9 deficiency in otherwise healthy children and adults with Candida species-induced meningoencephalitis, colitis, or both. *The Journal of allergy and clinical immunology*. 2015;135(6):1558-68.e2.
- 19. Hara H, Ishihara C, Takeuchi A, et al. The adaptor protein CARD9 is essential for the activation of myeloid cells through ITAM-associated and Toll-like receptors. *Nature Immunology*. 2007;8(6):619-29.
- 20. Grumach AS, de Queiroz-Telles F, Migaud M, et al. A Homozygous CARD9 Mutation in a Brazilian Patient with Deep Dermatophytosis. *J Clin Immunol*. 2015;35(5):486-90.
- 21. MacCallum DM, and Odds FC. Temporal events in the intravenous challenge model for experimental Candida albicans infections in female mice. *Mycoses.* 2005;48(3):151-61.
- 22. Black JT. Cerebral candidiasis: case report of brain abscess secondary to Candida albicans, and review of literature. *J Neurol Neurosurg Psychiatry*. 1970;33(6):864-70.
- 23. Croxford AL, Lanzinger M, Hartmann FJ, et al. The Cytokine GM-CSF Drives the Inflammatory Signature of CCR2+ Monocytes and Licenses Autoimmunity. *Immunity*. 2015;43(3):502-14.
- 24. Ngo LY, Kasahara S, Kumasaka DK, et al. Inflammatory monocytes mediate early and organ-specific innate defense during systemic candidiasis. *J Infect Dis.* 2014;209(1):109-19
- 25. Gazendam RP, van Hamme JL, Tool ATJ, et al. Two independent killing mechanisms of Candida albicans by human neutrophils: evidence from innate immunity defects. *Blood*. 2014;124(4):590-7.
- 26. Zajta E, Csonka K, Tóth A, et al. Signaling through Syk or CARD9 Mediates Species-Specific Anti-Candida Protection in Bone Marrow Chimeric Mice. *mBio*. 2021;12(4):e0160821.
- 27. Drewniak A, Gazendam RP, Tool ATJ, et al. Invasive fungal infection and impaired neutrophil killing in human CARD9 deficiency. *Blood.* 2013;121(13):2385-92.
- 28. Glocker EO, Hennigs A, Nabavi M, et al. A homozygous CARD9 mutation in a family with susceptibility to fungal infections. *N Engl J Med.* 2009;361(18):1727-35.
- 29. Clay H, Volkman HE, and Ramakrishnan L. Tumor Necrosis Factor Signaling Mediates Resistance to Mycobacteria by Inhibiting Bacterial Growth and Macrophage Death. *Immunity*. 2008;29(2):283-94.
- 30. Misme-Aucouturier B, Albassier M, Alvarez-Rueda N, et al. Specific Human and Candida Cellular Interactions Lead to Controlled or Persistent Infection Outcomes during Granuloma-Like Formation. *Infection and Immunity*. 2017;85(1):10.1128/iai.00807-16.
- 31. Drummond RA, Zahra FT, Natarajan M, et al. GM-CSF therapy in human caspase recruitment domain—containing protein 9 deficiency. *Journal of Allergy and Clinical Immunology*. 2018;142(4):1334-8.e5.
- 32. Wheeler RT, Kombe D, Agarwala SD, et al. Dynamic, morphotype-specific Candida albicans beta-glucan exposure during infection and drug treatment. *PLoS Pathog*. 2008;4(12):e1000227.

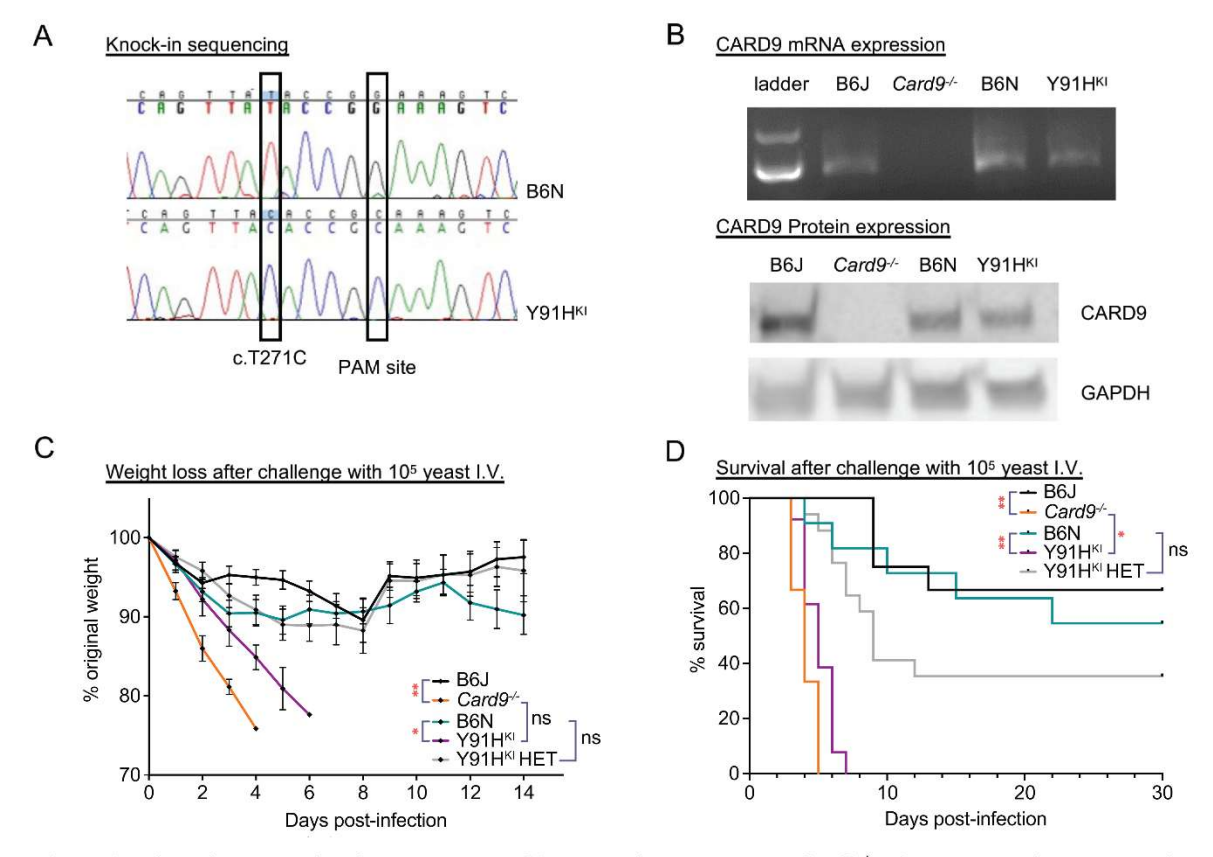


Figure 1. Mice with knock-in of the human p.Y91H mutation phenocopy *Card9*^{-/-} mice and are highly susceptible to disseminated candidiasis *in vivo*. A) Chromatograms of the Sanger sequencing of B6N and Y91H^{KI} mice showing the knock-in and associated silent PAM site mutation. B) RT-PCR showing *Card9* mRNA expression in BMDM and western blot for CARD9 protein with GAPDH as a loading control. Representative results of 2 experiments shown. C) Weight loss of mice injected via lateral tail vein with 1×10⁵ CFU of *C. albicans*. Multiple paired t tests for significance were performed. ns: no significance. *P<0.05, **P<0.01 in at least one time point. Mean and SEM shown. D) Kaplan-Meier survival curve of mice injected with 1x10⁵ *C. albicans* yeast I.V. *P < 0.05; **P < 0.01 by the Log-Rank Test. C&D) 3 experiments pooled. B6J: C57BL6/J, n=12 mice; *Card9*--: n=9 mice B6N: C57BL6/N, n=11 mice; Y91H^{KI}: mice homozygous for c.T271C, n=13 mice; Y91H^{KI} HET: mice heterozygous for c.T271C, n=17 mice.

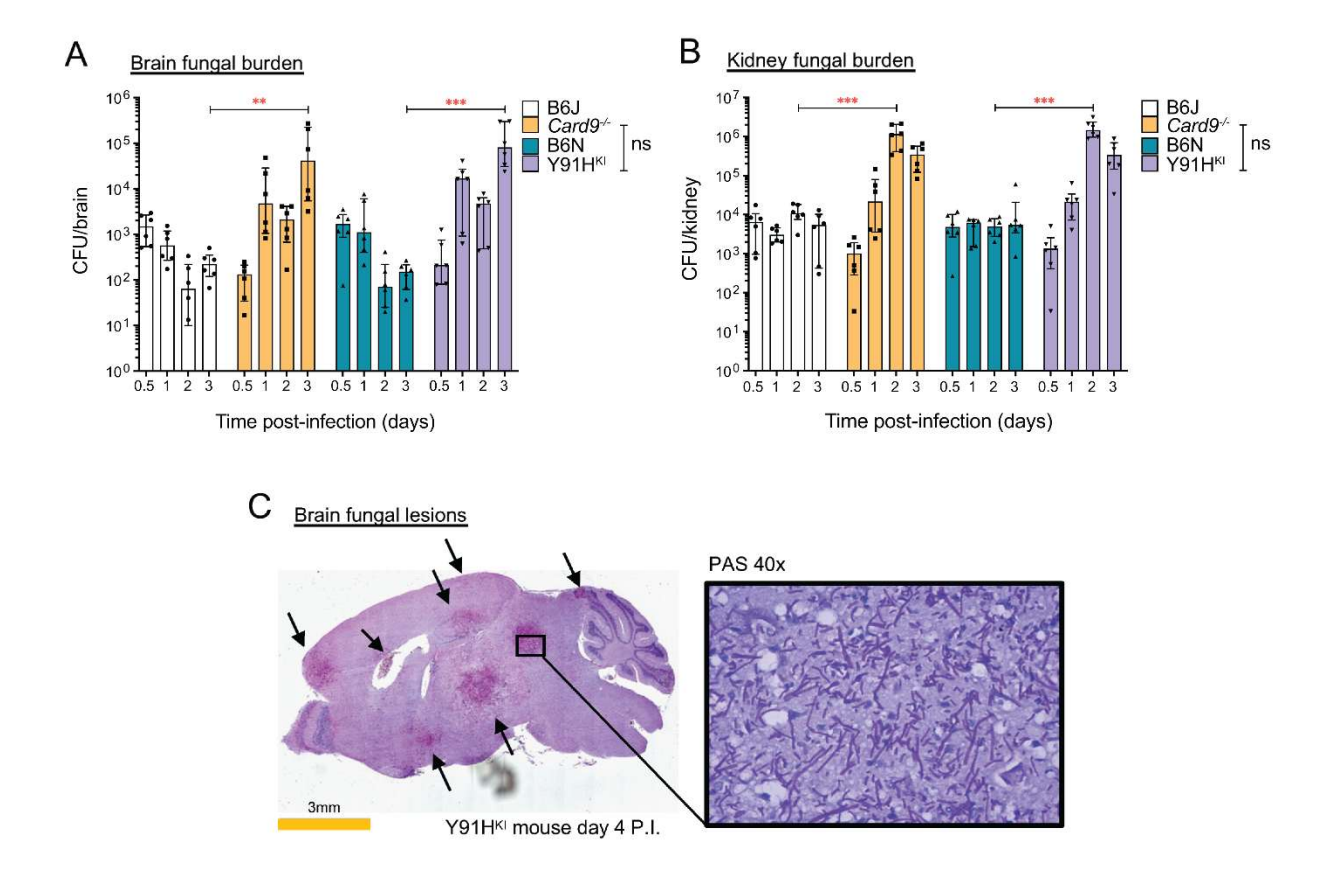


Figure 2. p.Y91H permits enhanced fungal growth in tissue and phenocopies Card9^{-/-} mice in susceptibility to disseminated disease after high dose C. albicans I.V. infection. A and B) Dot plots show tissue fungal burden from mice injected via lateral tail vein with 1×10⁵ C. albicans yeast cells. n=6 mice, 2 experiments pooled. Two-way ANOVA with Tukey's multiple comparisons test. **P<0.01, ***P<0.001, ns: not significant. Mean shown, error bars show SEM. C) Histopathology showing fungal lesions in the brain of Y91H^{KI} mice after 4 days of infection as for (A), stained with periodic acid schiff. Images were obtained by bright field microscopy with a 20x objective (whole brain) and 40x objective (zoom) and are representative of 2 experiments.

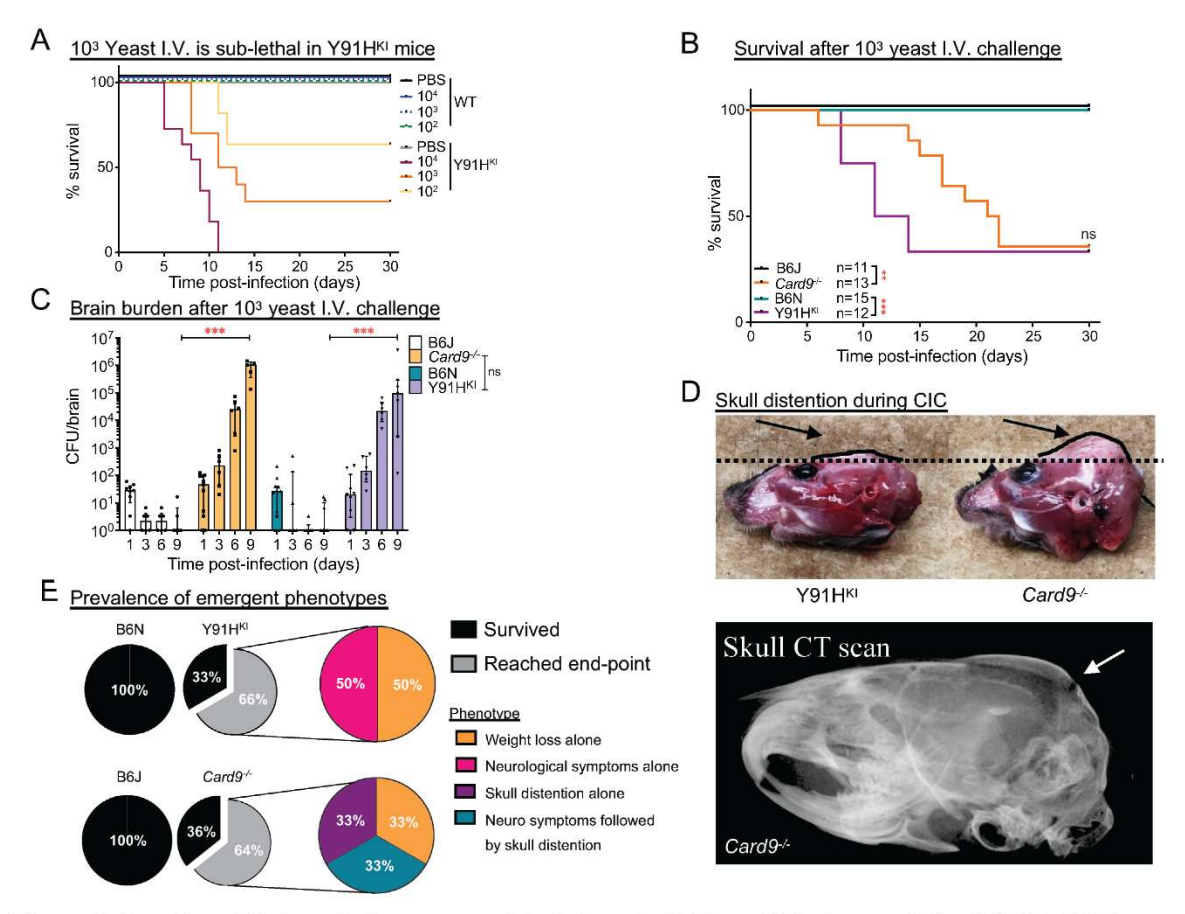


Figure 3. Low-dose I.V. inoculation as a model of chronic CNS candidiasis caused by CARD9-deficiency. A) Kaplan-Meier curve of mice infected with C albicans. B6N: n=6-8; Y91H^{KI}: n=8-13 mice per group, 2 experiments pooled. B) Kaplan-Meier curve of mice infected with 1×10^3 C. albicans. n=11-15 per group; 3 experiments pooled. *P < 0.05; **P < 0.01 by the Log-Rank Test. C) Brain burden after 1×10^3 C. albicans challenge. n=6-11 mice, 3 experiments pooled. Two-way ANOVA with Tukey's test. **P<0.01, ***P<0.001, mean and SEM shown. D) Representative images of skull distention. Gross comparison of the head of a Y91H^{KI} mouse that reached weight loss end-point and a $Card9^{-/-}$ mouse that reached end-point from severe skull distention and morbidity. Arrows and dotted line are visual aids. CT scan of a $Card9^{-/-}$ mouse skull at Day 22 P.I. with skull distention is shown. Arrows indicate areas where the skull has lost integrity. E) Prevalence of phenotypes observed in mice from (B). No symptoms were observed in surviving mice.

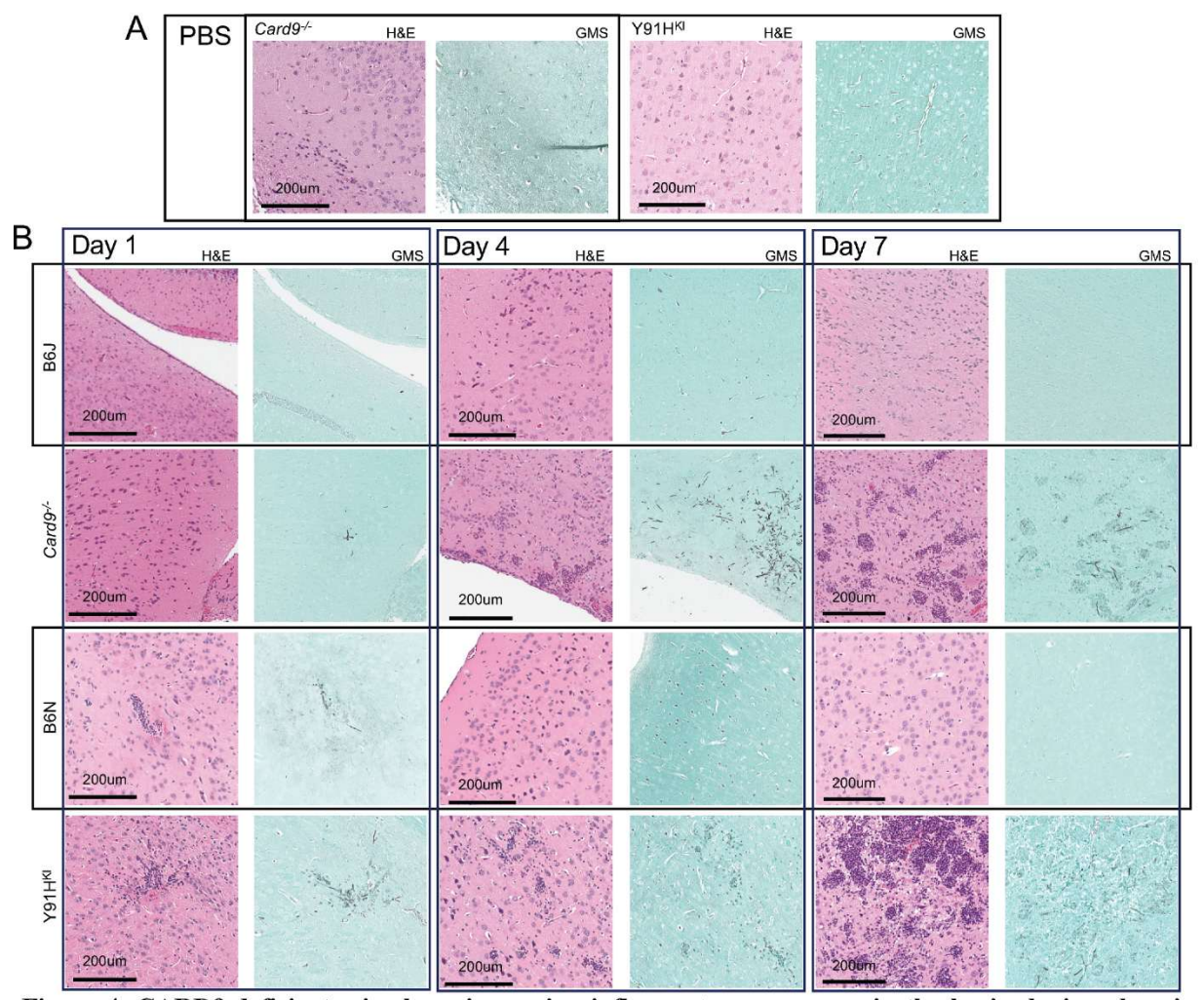


Figure 4. CARD9-deficient mice have increasing inflammatory responses in the brain during chronic invasive candidiasis. Histopathology staining of the brain. H&E (pink) and GMS (green) staining was done on serial sections. Images were obtained by bright field microscopy with a 20x objective and are representative of 2 experiments. A) PBS injected controls. B) Wild-type and CARD9-deficient mice at the indicated time points after infection with 1×10^3 C. albicans yeast cells. Scale bar shows 200microns.

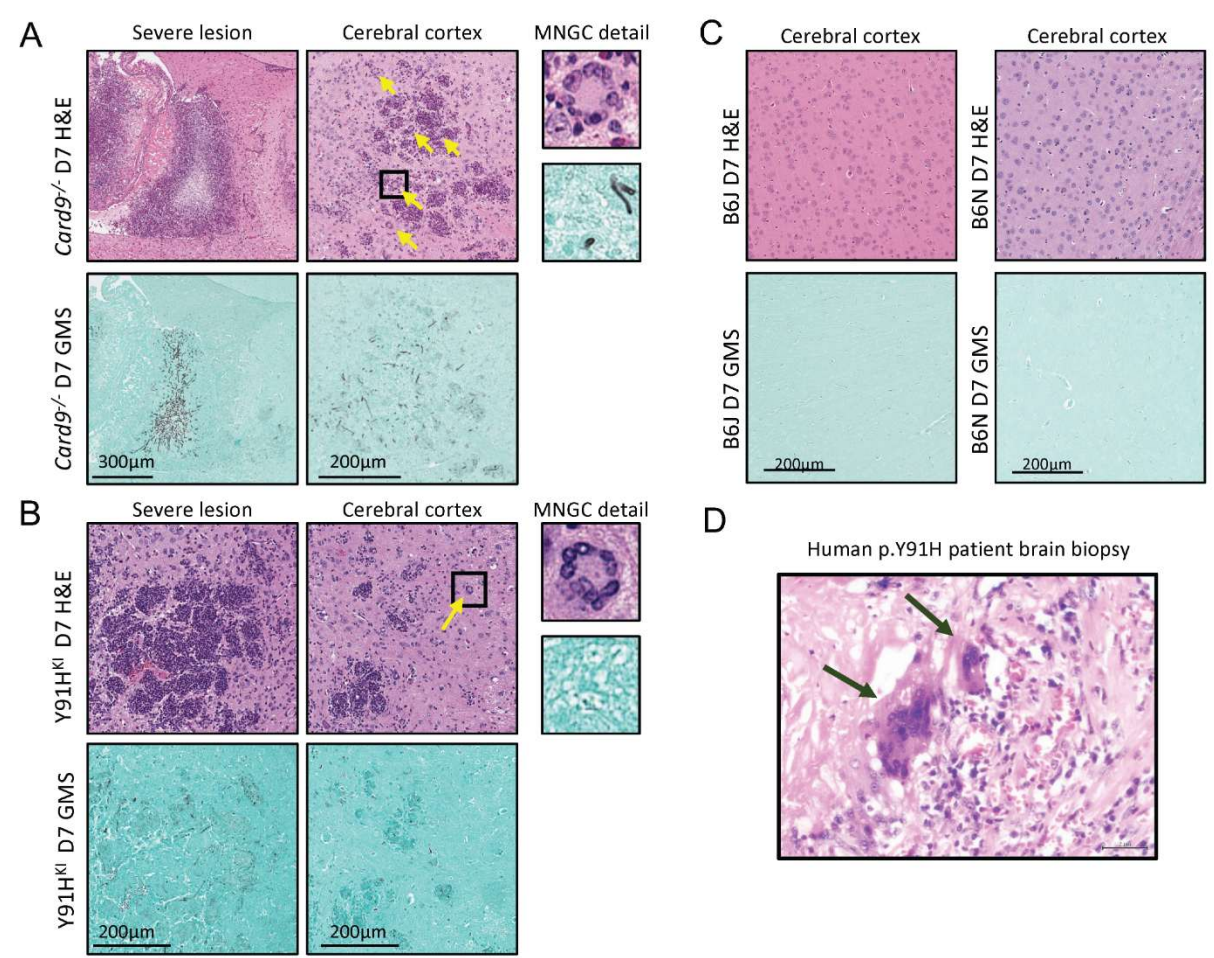


Figure 5. CARD9-deficient mice develop granulomatous inflammation with multinucleated giant cells. Histopathology staining of the brain of CARD9-deficient (**A**, **B**) and WT (**C**) mice at day 7 (D7) P.I. with 1x10³ *C. albicans* yeast cells. GMS and H&E staining were done on serial sections and images shown are matched for anatomical location. Yellow arrows indicate multinucleated giant cells (MNGC). Images were obtained by bright field microscopy with a 20x objective and are representative of 2 experiments. **D**) Human p.Y91H patient brain biopsy stained with H&E. Black arrows indicate MNGC. Microphotograph is 400x magnification; scale bar is 2microns. "Severe lesion" shows large histopathologic anomalies identified.

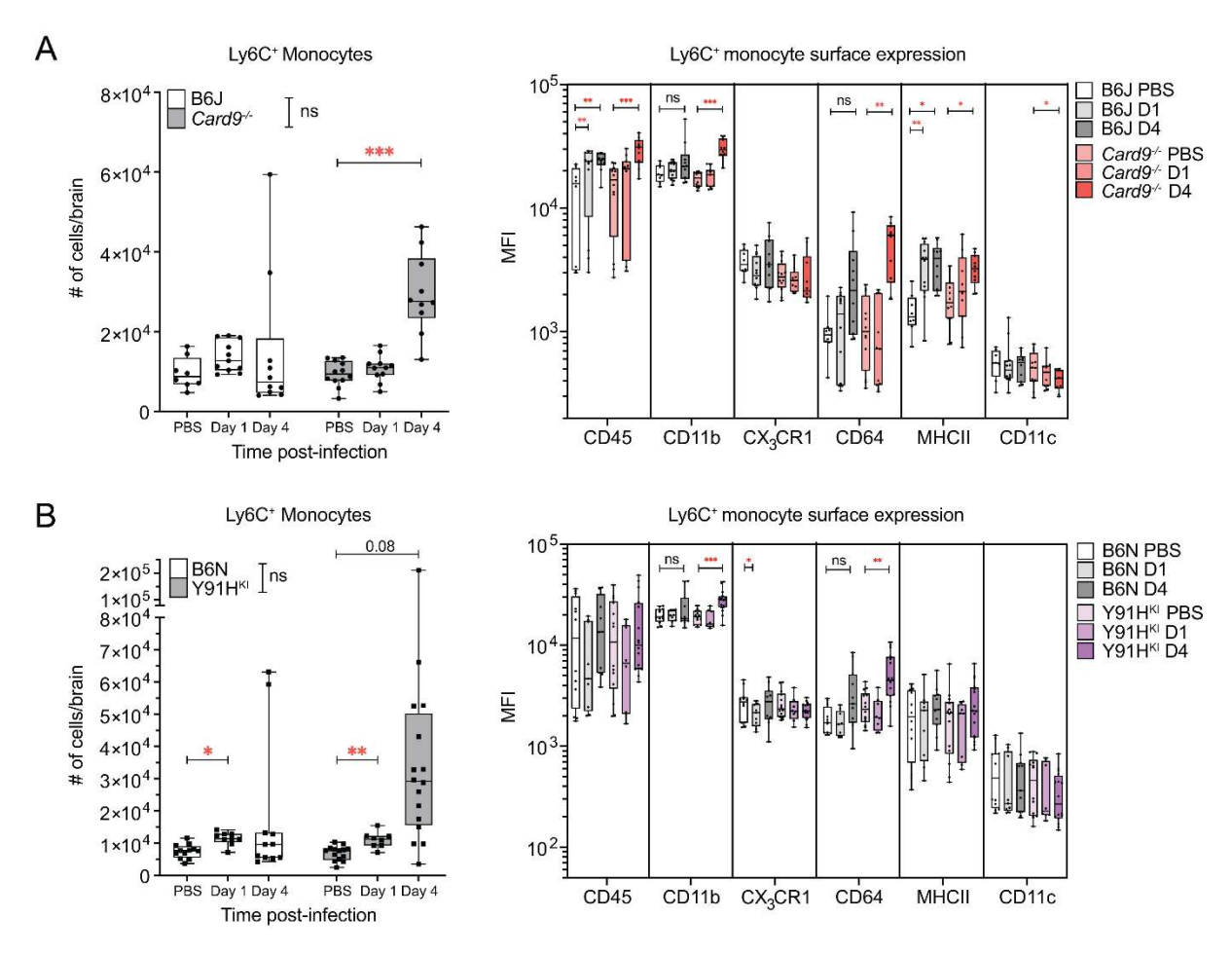


Figure 6. Monocytes and monocyte-derived dendritic cells accumulate in the brain during chronic invasive candidiasis. A) Box and whisker plots showing the number of inflammatory monocytes (CD45⁺CD11b⁺LIN⁻Ly6G⁻Ly6C⁺) and surface marker expression as MFI in the brain of B6J and *Card9*^{-/-} mice and **B)** in B6N and Y91H^{KI} mice. n=8-16 mice per group, 3 experiments pools. Median and interquartile range are shown. Two-way ANOVA with Dunnett's multiple comparisons test done for MFI. *P<0.05; **P<0.01; ***P<0.001.

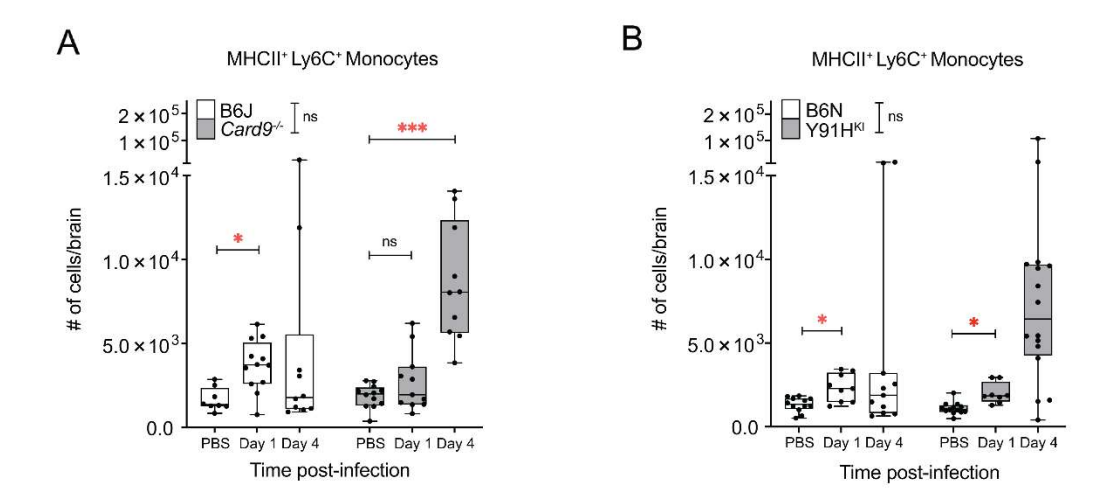


Figure 7. Monocyte-derived MHCII⁺ **cells accumulate in the brain during chronic invasive candidiasis. A)** Box and whisker plots showing the number of MHCII⁺ inflammatory monocytes (CD45⁺CD11b⁺LIN⁻Ly6G⁻Ly6C⁺MHCII⁺) in the brain of B6J and *Card9*^{-/-} mice and **B)** of B6N and Y91H^{KI} mice are shown. n=8-16 mice per group, 3 experiments pools. The median and interquartile range are shown. Two-way ANOVA with Tukey's multiple comparisons test. *P<0.05; **P<0.01; ***P<0.001.

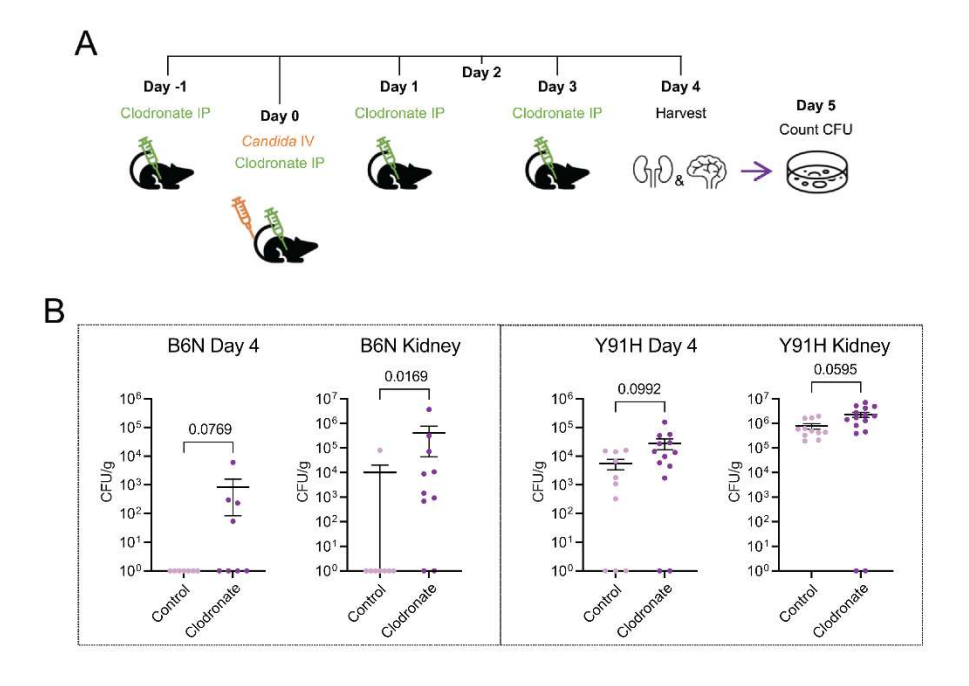


Figure 8. Mononuclear phagocytes are necessary for anti-fungal immunity in Y91H CARD9-deficiency A) Schematic of clodronate regime and infection. Mice were treated with control or clodronate as shown, and infected with $1x10^3$ C. albicans on day 0. Brain and kidney were harvested 4 days P.I. for enumeration of CFU. B) Brain and kidney fungal burden on day 4 P.I. Data was analyzed using the Mann-Whitney test and the P-value is indicated. n=8-15 mice per condition, 3 experiments pooled. Mean and SEM shown in black lines.

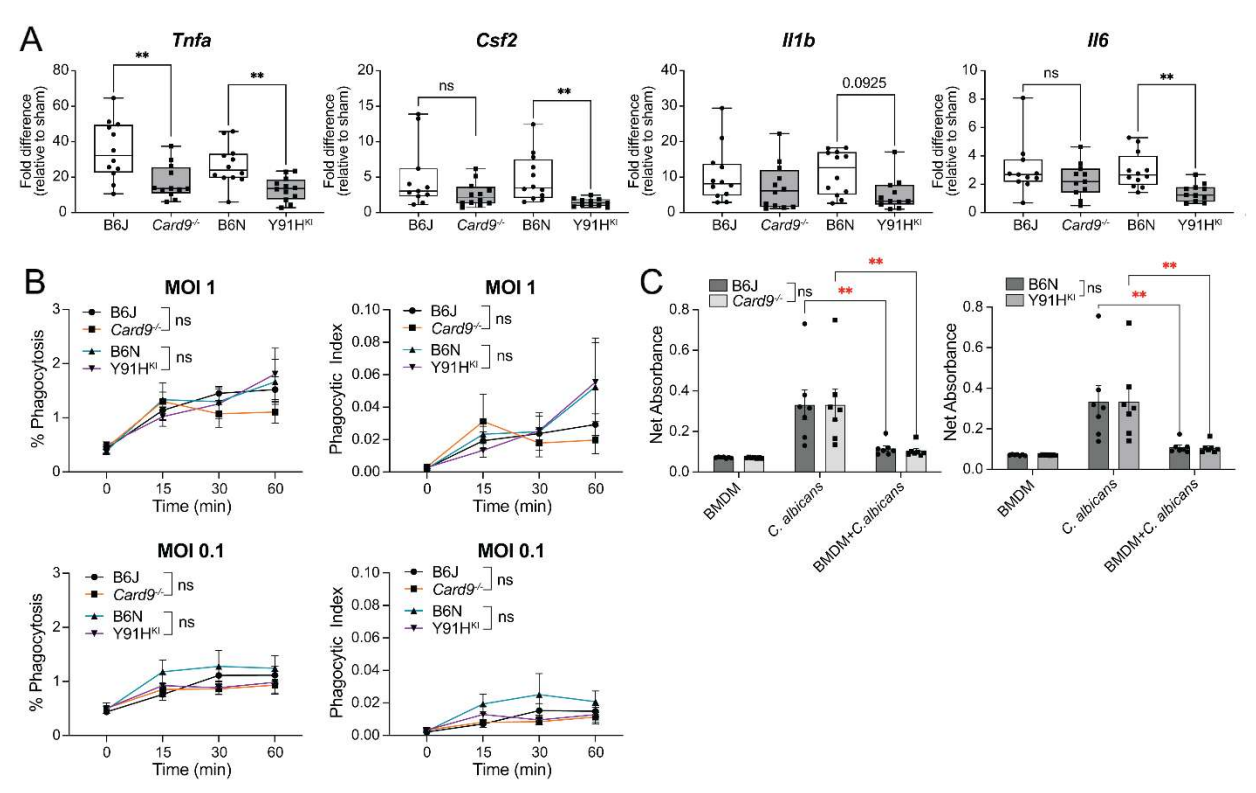


Figure 9. Impaired BMDM cytokine responses to live *C. albicans* in CARD9-deficiency. A) BMDM of each genotype were infected *in vitro* with live *C. albicans* yeast at an MOI 1 for 2hr. Cytokine expression by qPCR shown. n=12 mice per genotype, 7 experiments pools. Median and interquartile range shown. One-way ANOVA test for significance. B) BMDM were infected with GFP-tagged yeast cells at indicated MOI. Intracellular yeast enumerated at the times indicated by confocal microscopy. % phagocytosis = (# of BMDM with internalized yeast/total BMDM counted)x100. Phagocytic Index = (total # of engulfed yeast/ total # of counted BMDM) × (# of BMDM containing engulfed yeast/ total # of counted BMDM) × 100. n=9 mice per genotype, 3 experiments pooled, mean and SEM shown. C) BMDM alone, *C. albicans* alone, or BMDM infected with an MOI 0.1 for 6hr and an XTT assay performed. Net absorbance; n=6-7 mice, 3 experiments pooled; mean and SEM shown. Two-way ANOVA with Tukey's multiple comparisons test for significance. ns: not significant. *P<0.05; **P<0.01.

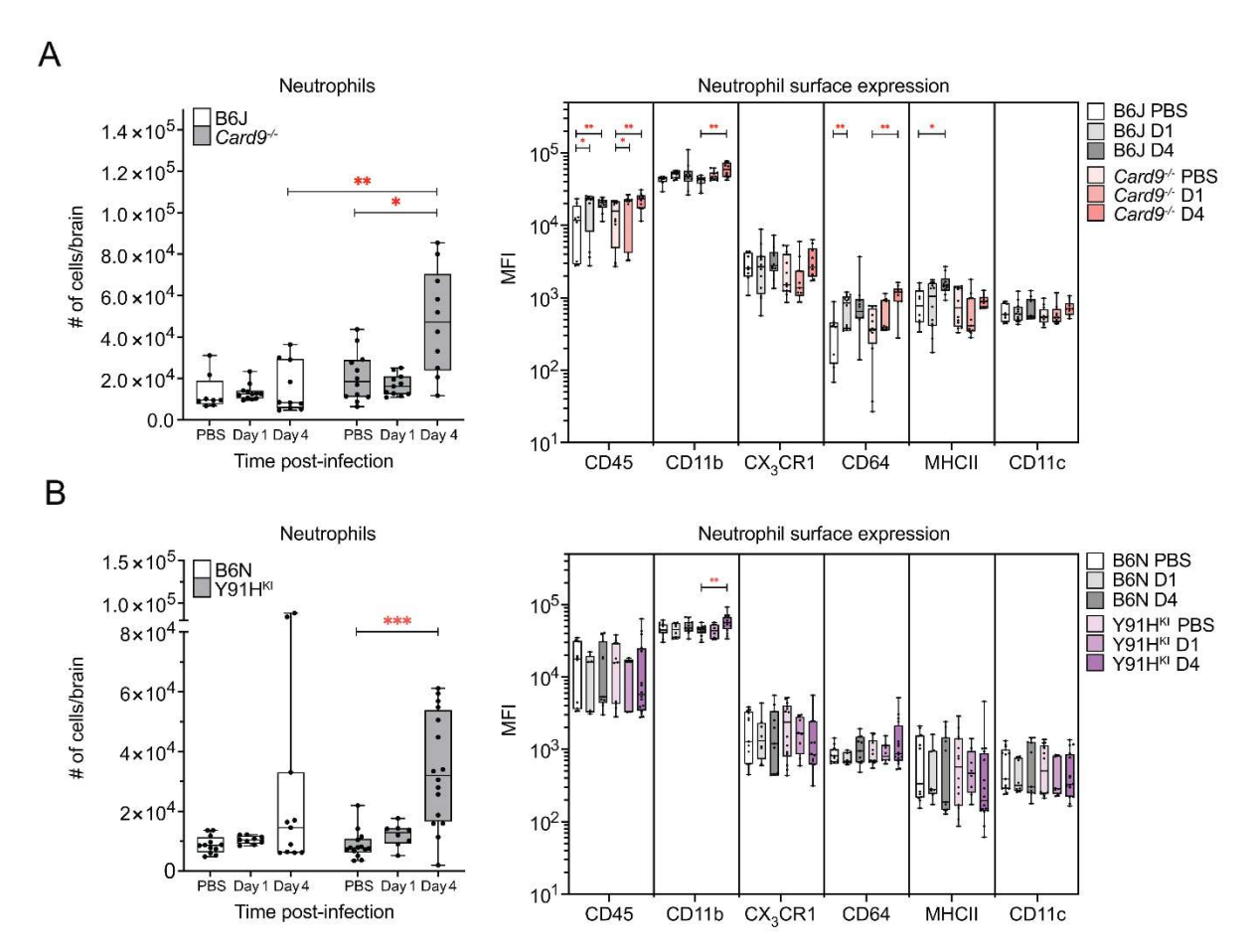


Figure 10. CARD9-deficient mice mount a neutrophil response in the brain during chronic invasive candidiasis. A) Box and whisker plots showing the number of neutrophils (CD45+CD11b+LIN-Ly6G+) and surface marker expression as MFI in the brain of B6J and *Card9-/-* mice and **B)** in B6N and Y91H^{KI} mice. n=8-16 mice per group, 3 experiments pools. Median and interquartile range shown. Two-way ANOVA with Dunnett's multiple comparisons test was used for MFI. *P<0.05; **P<0.01; ***P<0.001.